



HAL
open science

Tectono-Stratigraphic evolution of the Offshore Western Niger Delta from the Cretaceous to Present : Implications of Delta Dynamics and Paleo-Topography on Gravity-Driven Deformation

Kelvin Ikenna Chima, Didier Granjeon, Damien Do Couto, Marina Rabineau, Estelle Leroux, Christian Gorini, Jean Letouzey, Nick Hoggmascall, Miguel-Mora Glukstad

► To cite this version:

Kelvin Ikenna Chima, Didier Granjeon, Damien Do Couto, Marina Rabineau, Estelle Leroux, et al.. Tectono-Stratigraphic evolution of the Offshore Western Niger Delta from the Cretaceous to Present : Implications of Delta Dynamics and Paleo-Topography on Gravity-Driven Deformation. Basin Research, 2022, 34 (1), pp.25-49. 10.1111/bre.12609 . hal-03700016

HAL Id: hal-03700016

<https://ifp.hal.science/hal-03700016>

Submitted on 20 Jun 2022

HAL is a multi-disciplinary open access archive for the deposit and dissemination of scientific research documents, whether they are published or not. The documents may come from teaching and research institutions in France or abroad, or from public or private research centers.

L'archive ouverte pluridisciplinaire **HAL**, est destinée au dépôt et à la diffusion de documents scientifiques de niveau recherche, publiés ou non, émanant des établissements d'enseignement et de recherche français ou étrangers, des laboratoires publics ou privés.

Title

Tectono-stratigraphic evolution of the offshore western Niger Delta from the Cretaceous to present: Implications of delta dynamics and paleo-topography on gravity-driven deformation

Authors

Kelvin Ikenna Chima (1,2), Didier Granjeon (3), Damien Do Couto (1), Estelle Leroux (4), Christian Gorini (1), Marina Rabineau (5), Jean Letouzey (1), Nick Hoggmascall (6), Miguel-Mora Glukstad (7)

(1) Sorbonne Université-ISTeP UMR 7193, Paris, France

(2) Alex Ekwueme Federal University, Ndufu-Alike, Abakaliki, Nigeria

(3) IFPEN, Rueil-Malmaison, France

(4) IFREMER, ZI Pointe du Diable, Plouzane, France

(5) Laboratoire Géosciences Océan (LGO), UMR6538, CNRS, Univ Brest, Univ. Bretagne-Sud, IUEM, Plouzané, France

(6) Brunei Shell Petroleum Sendirian Berhad, Panaga, Brunei

(7) Ras Al Hamra Petroleum Development Oman (PDO), Muscat, Oman

Abstract

The interaction between sedimentary wedge dynamics and paleo-fracture zones is investigated offshore western Niger Delta lobe (WNDL) to reconstruct the evolution of the delta from the Cretaceous to present. This was achieved through detailed regional seismic interpretation, calibrated with well data. Our results suggest that high sedimentation rates in the WNDL since the Serravallian–Tortonian triggered the migration of the ‘Oligocene-Tortonian extensional zone’ and gravity spreading seawards (from a present-day onshore to a present-day offshore position), with extensional, translational and contractional deformation. An additional increase in sedimentation rate since the early Pliocene, further accelerated gravity spreading and the development of the present-day contractional front. A five-stage tectono-stratigraphic evolution of the offshore WNDL from the late Cretaceous to present is proposed. Paleo-topographies formed by the Charcot and Chain Fracture Zones exerted depositional control on the stratigraphic architecture of the offshore WNDL from the Cretaceous to Serravallian. Differential subsidence on both sides of the relict Charcot and Chain transform faults is responsible for the segmentation of gravity-driven deformation of the eastern and western Niger Delta lobes. In addition, a comparison of the stratigraphic architecture of the eastern Niger Delta lobe (ENDL) and WNDL demonstrates a similar overall progradation and sediment bypass

to the deep basin during the Pliocene. During the Pleistocene, the two lobes show a distinct evolution and architecture: the ENDL shows an overall retrogradation and sediment sequestration on the shelf, whereas the WNDL displays an overall progradation and sediment bypass. This study documents long-term and large-scale control of delta dynamics and paleo-topography on gravity-driven deformation of the offshore eastern and western Niger Delta lobes, and similar analysis could be applied in the reconstruction of other passive margin basins.

1. Introduction

The Cenozoic Niger Delta is a prolific petroleum province, fed by a large progradational delta along a passive continental margin. The Niger Delta is characterised by gravity-driven deformation of a sedimentary wedge above overpressured marine shales (Cohen & McClay, 1996; Damuth, 1994; Doust & Omatsola, 1990; Figure 1). The siliciclastic wedge of the Niger Delta is ca. 12 km thick, and displays concave, divergent seaward lobate geometry in plan view (Figure 1b). The main pulse of deltaic sedimentation started in the late Eocene and the delta front has prograded ca. 300 km seaward of the modern coastline (Figure 1b,c). Gravity-driven deformation of the Niger Delta wedge is characterised by delta-top extensional faults in the proximal setting and imbricated fold-thrust faults that detach within overpressured marine shales in the distal setting (Figure 1b,c).

The offshore Niger Delta is segmented into the eastern Niger Delta lobe (ENDL) and western Niger Delta lobe (WNDL) by stepped oceanic basement, formed by the Charcot Fracture Zone (Evamy et al., 1978; Short & Stauble, 1967; Wu et al., 2015; Figure 1a,b). The ENDL and WNDL are, in turn, underlain by Fernando Po and Chain Fracture Zones respectively (Figure 1a,b). These fracture zones were active transform faults in the middle Aptian, during the opening of the equatorial Atlantic, but were fossilised in the Santonian, when oceanic spreading began to slow down (Briggs et al., 2009; Lehner & de Ruiter, 1997). Although analogue modelling of the offshore Niger Delta by Wu et al. (2015) documented differential sediment thickening across the relict Chain and Charcot Fracture Zones, the long-term effects of these features remain undetermined. The relict Chain and Charcot Fracture Zones have been shown to have controlled the stratigraphic architecture of the adjacent margins of Ghana and Ivory Coast due to their proximity to these regions (de Matos, 2000). The relict Chain and Charcot Fracture Zones, as well as buried volcanoes (hotspots), have also been shown to play the role of buttressing or concentrating strain at the toe of the Niger Delta lobe (Briggs et al., 2009; Davies et al., 2005). For example, the Charcot Fracture Zone provides a prominent separation between the ENDL and WNDL (Figure 1a,b), while faults above the Chain Fracture Zone have linked to strain localisation (Cobbold et al., 2009; Morgan, 2004). In the WNDL, the Chain and Charcot Fracture Zones are oriented

oblique/parallel to the modern continental slope (Figure 1a,b), and serve as transfer zones and control the position of submarine channels (Krueger & Grant, 2011).

Gravity-driven deformation on passive margins is generally dominated by gravity gliding and gravity spreading (Dejong & Scholten, 1973; Ramberg, 1981; Schultz-Ela, 2001). Gravity gliding is defined as a rigid, downward movement of sediment along a basal slip surface (regional detachment), while gravity spreading is defined as the lateral extension and vertical contraction of a linked system, regardless of basal slope or coherence of the system (Schultz-Ela, 2001). Gravity spreading has been identified as the main mechanism of deformation of the Niger Delta's sedimentary wedge (Cobbold et al., 2004; Peel, 2014; Rowan et al., 2004; Wiener et al., 2010; Wu et al., 2015). However, the timing and kinematics of deformation remain poorly understood. Gravity spreading of the WNDL is driven by the presence of seaward-dipping bathymetric surface and high sedimentation/progradation rate of deltaic sediments above overpressured marine shales (see review in Morley et al., 2011; Figure 1c). Rapid burial of sediments at ca. 4 km beneath overburden, and differential compaction at ca. 4 km deep, result to overpressure within the shales, facilitating gravity-driven deformation (Briggs et al., 2006; Doust & Omatsola, 1990; Morgan, 2004; Wiener et al., 2010; Figure 1c).

Despite numerous studies of the offshore WNDL over the past decade, the interplay of delta dynamics and paleotopography as controls on gravity-driven deformation over the entire Niger Delta since the Cretaceous remains poorly understood. This is investigated in this study with specific focus on the Pliocene and the Pleistocene stratigraphic architecture of the offshore WNDL (Figure 1), which is compared with the well-documented ENDL.

2. Regional setting

The Niger Delta is located in the Gulf of Guinea on the equatorial Atlantic margin of West Africa (Figure 1). The unique tectono-stratigraphic setting of the Niger Delta has attracted both the industry and the academic investigations over the past decades as a natural laboratory to study (a) regional/global climate dynamics; (b) sea-level changes; (c) gravity-driven deformation; (d) evolution of river catchments and (e) their control on sediment supply, distribution and overall stratigraphic architecture of a large progradational delta on passive continental margin (Jermannaud et al., 2010; Rouby et al., 2011).

Recent studies by Chardon et al. (2016) and Grimaud et al. (2017) demonstrated that the modern Niger catchment developed during the late Eocene–early Oligocene (ca. 34–29 Ma), following a regional magmatic upwelling of the northern part of the region. Chardon et al. (2016) and Grimaud et al. (2017)

also showed that the magmatic upwelling triggered the re-organisation of the Niger catchment, with an overall increase in sediment supply to the offshore Niger Delta.

Wiener et al. (2010) demonstrated that the Niger Delta's 'Oligocene-Tortonian extensional zone' is in the present-day onshore (Figure 1b), but was in the offshore at the time of deposition. During the Tortonian (ca. 9.3 Ma), an overall increase in sedimentation triggered the seaward progradation of passive margin slope, burial of the 'Oligocene-Tortonian extensional zone' and the development of the extensional zone seawards (Figure 1b). An additional increase in sedimentation was also documented in the offshore Niger Delta between the early Pliocene (5.3 Ma) and the early Pleistocene (1.8 Ma) (now 2.6 Ma; Gibbard et al., 2014) (Grimaud et al., 2017; Haack et al., 2000; Robin et al., 2011). The ENDL records progradation with an overall increase in sedimentation between ca. 4 and ca. 2.5 Ma, and retrogradation with an overall decrease in sedimentation onwards to present-day. Jermannaud et al. (2010) attributed the overall reduction in sedimentation in the ENDL to: (a) a regional migration of delta lobe/switch of sediment fluxes from the ENDL to the WNDL or (b) a climatic warming of west Africa/aridification of the Niger catchment led to an overall decrease in sediment supply in the entire Niger Delta.

The lithostratigraphy of the Niger Delta comprises the contemporaneous Akata, Agbada and Benin formations (Avbovbo, 1978; Doust & Omatsola, 1990; Figure 1d). The 3to 4-km-thick sediments of the Akata Formation comprise parallel-laminated marine muds/shales, which ranges between Paleocene–recent, and generally is considered as the principal source rock (Avbovbo, 1978; Haack et al., 2000; Figure 1d). The Akata Formation serves as the root of overpressure in the Niger Delta (Haack et al., 2000; Figure 1d). The 2to 9-km-thick deltaic sediments of the Agbada Formation range between the Eocene-recent, and serve as reservoir/source-seal (Avbovbo, 1978; Doust & Omatsola, 1990; Haack et al., 2000; Figure 1d). The 2-km thick fluvial to upper coastal plain sediments of the Benin Formation range between the Miocene–recent (Avbovbo, 1978, Figure 1d). Gravity-driven deformation of the Niger Delta's sedimentary wedge since the late Eocene resulted in the development of three structural zones, namely: (a) an extensional zone, dominated by seaward and landward-dipping, normal faults; (b) a translational zone, dominated by thrust/shale-cored anticlines and shale-withdrawal intraslope basins and (c) a contractional zone, dominated by imbricated thrust sheets and associated folds (Cohen & McClay, 1996; Doust & Omatsola, 1990; Morgan, 2004; Figure 1c). Regional seismic observations, and analogue and numerical models, show that the deformation of sediments in these structural zones is generally complicated by the presence of multiple detachments (Bellingham et al., 2014; Briggs et al., 2006; Corredor et al., 2005; Peel, 2014; Restrepo-Pace, 2018; Sapin et al., 2012; Wiener et al., 2010; Figure 1c).

3. Dataset and methodology

3.1 Seismic and well data

We combined seismic reflection and well data to study the tectono-stratigraphic evolution of the offshore western Niger Delta from the Cretaceous to present. Seismic reflection data comprised 21 widely spaced 2D lines (6 strike lines and 15 dip lines), which cover an area of ca. 4,120 km² on the continental shelf (Figure 1b). Among these lines, one 500-km-long strike line extends throughout Niger Delta lobes (see the red line labelled Figure 6 in Figure 1b). Others lines include three regional dip lines that extend beyond the continental shelf, with the longest (>200 km), reaching the abyssal plain (see the red lines labelled Figures 3, 4/10b and 5 in Figure 1b). The seismic reflection data were processed as zero-phase source wavelet in the American reverse standard polarity such that an increase in acoustic impedance corresponds to a trough (black loop) in the wavelet, while a decrease in acoustic impedance is represented by a peak (white loop). They are characterised by a sampling interval of 4 ms two-way travel time (TWT) and vertical resolution, which ranges between 25 and 40 m.

We analysed a total of 20 wells (15 on the continental shelf and 5 on the continental slope; Figure 1b; Table 1). The wells on the continental shelf were labelled Izaga shelf (IZSH 1 to IZSH 15) (Figure 1b; Table 1). The wells on the slope that were previously labelled as FM-1 to FM-5 in (Chima et al., 2019) were labelled in this study as FMSL 1 to FMSL 5 (SL for slope; Figure 1b; Table 1) to distinguish them from the shelf wells. While FMSL 1 to FMSL 5 generally provide gamma ray, resistivity, neutron, density and sonic logs, only IZSH 1, 4, 7, 13 and 15 had gamma ray, resistivity, neutron, density or sonic logs (Table 1). FMSL 1 to FMSL 5 and IZSH 1, 2, 4, 6, 7, 11, 14 and 15 also had checkshot data (Table 1). Biostratigraphic studies were also available for FMSL 1 to FMSL 4 wells (see figs. 2, 7 and 8 in Chima et al., 2019), and were used to date the entire Neogene, from the Burdigalian to Messinian, on the continental slope. The Pliocene and the Pleistocene sedimentary records generally lack biostratigraphic data. Of the 15 wells on the continental shelf, only IZSH 1, 4, 7, 13 and 15 contain biostratigraphic data for the Messinian interval (Table 1). Also, of the eight seismic surfaces that were identified on the continental slope (see Chima et al., 2019; Figure 1b), only three surfaces (the Serravallian, Tortonian and Messinian) could be correlated up-dip to the continental shelf. The inferred early Pliocene, early Pleistocene and middle Pleistocene seismic surfaces (see fig. 10 in Chima et al., 2020) were also correlated up-dip to the continental shelf. The age of an older seismic surface (the late Eocene), which was not penetrated by the wells that we studied, was estimated from Bellingham et al. (2014; Figure 1c).

3.2 Methodology

3.2.1 Seismic stratigraphy

This study builds on the recently published sequence stratigraphic and cyclostratigraphic studies of the 3D seismic survey located on the western Niger Delta continental slope (see figs. 5 and 10 in Chima et al., 2019, 2020) respectively. These studies applied the sequence stratigraphic approach described by Mitchum and Vail (1977), which combines the recognition of amplitudes of seismic reflection, continuity, internal architecture, external geometry, nature of bounding surfaces and erosional truncations. Seismic stratigraphy was calibrated with detailed 3D seismic geomorphological analysis to delineate key sequence stratigraphic surfaces (see figs. 5, 10 and 12 in Chima et al., 2019). Detailed analysis of calcareous nannofossil and planktonic foraminifera data from FMSL 1–4 were used to date stratigraphic surfaces from the Burdigalian to the Messinian (see figs. 5, 7 and 8 in Chima et al., 2019 for a more detailed explanation).

Despite the abundance of wells on the continental shelf (Figure 1b; Table 1), their general lack of biostratigraphic data did not allow the direct calibration of the ages of the five stratigraphic surfaces identified in this region. However, this challenge was overcome by extending the eight biostratigraphic and cyclostratigraphic surfaces (combined), identified on the continental slope (see Chima et al., 2019, 2020), down-dip to the abyssal plain and updip to the continental shelf. This was achieved with the aid of six interconnecting, regional 2D seismic lines (see the red lines in Figure 1b). The general decrease in the vertical resolution of seismic data at depths >3.5 s TWT, coupled with the abundance of growth faults and their associated shadow zones, locally hampered stratigraphic correlation notably in the outer shelf. However, signal processing algorithms in Petrel™ software (median filter and structural smoothing), as well as reflection matching using 'ghost method', helped to improve the overall reflection continuity and aid seismic interpretation. Although we followed the conventional rules and meticulously interpreted our data, we are aware that the level of uncertainty in the correlation of stratigraphic surfaces across major growth faults, and laterally away, may be up to 50 m.

3.2.2 Velocity analysis, time-depth conversion and estimates of average sedimentation rates

After a detailed quality control of the checkshot data of five wells (FMSL 1–5; Figure 1b, Table 1), we carried out the analysis of average velocity (m/s) versus measured depth (m) on the deepest FMSL 1 well, which was drilled to a total depth of 4,154 m (see figs. 2 and 7 in Chima et al., 2019). We used the 'layer cake' approach in which we first defined stratigraphic units identified in the seismic data

(Figure 2). We plotted average velocity (V_{avg}) versus measured depth (MD), and used a linear regression to define the relationship between velocity and depth for each stratigraphic unit (Figure 2). The slope (K) and intercept (V_o) of this linear relationship ($V = KZ + V_o$) made it possible to build a time-to-depth conversion model. FMSL 1 well only sampled the uppermost part of the late Eocene-Burdigalian Unit (Figure 2). Therefore, we extrapolated the linear function using velocity-depth information estimated from a published line, a few kilometres from this study (see Bellingham et al., 2014: Figure 1b,c). This allowed us to obtain a consistent linear function down to the late Eocene surface (Figure 2). We converted TWT surfaces to depth surfaces starting from the seafloor (the reference depth), using Petrel™ software.

Due to the widely spaced nature of the 2D seismic lines, estimates of average sediment thickness and average sedimentation rates were made on key regional seismic profiles (Figure 1b). Average sedimentation rates were estimated on the seismic lines (labelled Figures 4/10b and 5 in Figure 1b). This was achieved by measuring the present-day surface area (km²) of each key stratigraphic unit, defined as a faulted polygon (length and height in kilometres). This surface area was divided by the length (km) of the seismic lines to obtain the average sediment thickness (km) of each unit. This average sediment thickness was, in turn, divided by the duration of deposition (Ma) of the unit to obtain average sedimentation rates (km/Myr).

The main uncertainty in the above workflow (velocity model, estimates of average sediment thickness and depositional rates) is that it was entirely based on the deepest FMSL 1 well on the continental slope. This is due to the lack of wells in the deep basin, and the ones on the continental shelf have a limited penetration or lack checkshot data (Figures 1b,c and 2; Table 1). Secondly, due to the lack of checkshot data within the first 1,378 m and below 4,050 m, velocity-depth plots in these intervals were based on extrapolation and information from a published study (see Bellingham et al., 2014; Figure 1b,c). The overall poor seismic reflectivity within the deeper stratigraphic intervals (e.g. the late Eocene–Serravallian), across major growth faults and imbricated thrusts, locally impacted seismic interpretation, estimates of average sediment thickness and depositional rates. Estimated average sediment thickness and depositional rates were based on selected, widely spaced 2D lines, which do not represent the entire offshore WNDL. Regardless of the foregoing challenges and the overall shallowing of the stratigraphic surfaces above the Pleistocene, below the Burdigalian and away from the continental slope, we obtained depth profiles, stratigraphic thicknesses and depositional rates that are comparable with published studies.

4. Results

4.1 Stratigraphic units

We extended the previously identified stratigraphic units from the continental slope (see Chima et al., 2019, 2020), up-dip to the continental shelf and down-dip to the deep basin (see the red lines in Figure 1b). The correlation of stratigraphic surfaces across regional, depth-penetrating 2D seismic lines (Figure 1b), allowed us to investigate the control of delta dynamics and paleo-topography on gravity-driven deformation of the offshore WNDL since the Cretaceous (Figures 3–6 and 8).

4.1.1. The late Cretaceous–late Eocene Unit

Description

The late Cretaceous–late Eocene Unit is the oldest stratigraphic unit identified in the offshore WNDL (Figures 3–5). It is bounded at the base and top by moderate-to-high-amplitude seismic reflections (marked in dark green and light blue respectively; Figures 3, 4a and 5a). The Cretaceous and late Eocene ages, assigned to these seismic reflectors, were based on comparison of our seismic lines (Figures 3 and 4) with that of Bellingham et al. (2014; Figure 1c). The late Cretaceous surface (labelled TB in Figures 3–6) caps the underlying, acoustic seismic unit, marked by chaotic, moderate-to-high-amplitude seismic reflections. This acoustic seismic unit is locally overlain in the WNDL by a wedge-shaped, high-amplitude seismic reflections, highlighted in yellow in Figure 6a,b. A moderate-to-high-amplitude seismic reflector (labelled RD in Figures 3, 4a and 5a), at the middle part of the late Cretaceous–late Eocene Unit, sub-divides the unit into two low-reflectivity sub-units (labelled LDU and UDU in Figures 3–5). The LDU and UDU are highlighted in light and dark grey respectively (Figures 4b and 5b). The late Cretaceous–late Eocene Unit generally decreases in thickness seaward, with its upper sub-unit, displaying remarkable thickness within the translational zone and the inner-fold-thrust belt (IFTB), where linear features characterised by listric geometries are common (Figures 3–5). The late Cretaceous–late Eocene Unit reaches an average thickness of 1.8 and 2.1 km in Figures 4 and 5 respectively. On a delta-wide strike line located on the continental shelf (Figures 1a and 6), the late Eocene surface interpreted on the regional dip lines (Figures 3–5) could not be identified due to seismic wipe-out (Figure 6a). The poor reflectivity seismic unit (the interval highlighted in red in Figure 6b) displays a remarkable lateral variation in thickness with an average of 1.2 km. The unit generally thins at the crests of paleo-structural highs in the central and western Niger Delta (Figure 6a,b). Linear features that offset seismic reflections are distributed throughout the deltawide strike line, and are poorly imaged within the deeper stratigraphic intervals (Figure 6). On regional dip lines (Figures 3–5),

these linear features display high angles of inclination within the younger stratigraphy, but develop listric geometry within the deeper stratigraphy. These linear features generally terminate at oblique angles on the regional seismic surface (labelled RD in Figures 3–5). In map view, these linear features measure between 50 and 100 km in length, with parallel to sub-parallel geometry to the modern coastline (Figure 1b). They range in dip orientation from dominantly landward in the ENDL to dominantly seaward towards WNDL (Figure 1b).

Interpretation

The seismic unit, characterised by chaotic, moderate– high-amplitude reflectors, bounded at the top by a high-amplitude seismic reflector, is interpreted as the acoustic basement (Figures 3–6). The paleo-structural highs identified in the central and western Niger Delta are interpreted as the Charcot and Chain Fracture Zones respectively (see Evamy et al., 1978; Short & Stauble, 1967; Figures 1a,b and 6a,b,d,e). The wedge-shaped, high-amplitude reflectors, which overlie the Chain Fracture Zone to the west, are interpreted as syn-rift deposits (Figure 6a,e). The lateral variation in thickness of the reflection-free seismic unit (highlighted in red in Figure 6b), with an overall thinning at the crests of the Charcot and Chain Fracture Zones, indicate that these paleo-topographies exerted depositional control on the geometry of the unit. The reflection-free seismic units (labelled LDU and UDU in Figures 3–5), which overlie the basement, are interpreted as lower and upper detachment units respectively (see Bellingham et al., 2014; Figure 1c). The moderate-to-high-amplitude seismic reflector (labelled RD in Figures 3–5), which delimits the lower and upper detachment units, is interpreted as a regional detachment/décollement (see also Bellingham et al., 2014; Figure 1c). This interpretation is supported by the termination of most linear features on this surface (Figures 3–5). The normal and reverse offsets of seismic reflectors across linear features support the presence of normal and thrust faults respectively (Figures 3–5). The bathymetric highs (labelled BH in Figures 4 and 5) are interpreted as thrust/mobile shale-cored anticlines. The negative topographies that flank the thrust/shale-cored structures are interpreted as intraslope basins (ISBs) (see also Adeogba et al., 2005; Bakare et al., 2007; Chima et al., 2019, 2020; Prather et al., 2012; Figure 4b). The reflection-free interval (highlighted in red in Figure 6b), where the late Eocene and the Burdigalian surfaces could not be tracked (Figure 6a), suggests burial of sediment below the resolution of our seismic data. The overall thickening of the UDU within the translational zone and IFTB is interpreted as structural thickening linked to duplexing (Figures 4 and 5). Duplexing could also be responsible for the thickening of the LDU within the translational zone and IFTB (see also Jolly et al., 2016; Figure 4b).

4.1.2 The late Eocene – Serravallian Unit

Description

The late Eocene–Serravallian Unit is bounded at the base and top by undulating, moderate-to-high-amplitude seismic reflectors, highlighted in light blue and black in Figures 3–5. This seismic reflector marks a transition from the underlying transparent unit to the overlying, moderate-to-high-amplitude seismic reflectors (Figures 3–5). The unit is marked in the middle by an undulating seismic reflector, which was dated as Burdigalian by Chima et al. (2019) using biostratigraphic data (see the pink horizon in Figures 3–5). The late Eocene–Serravallian Unit displays a total average thickness of 0.46 km, comprising 0.25 km for the late Eocene–Burdigalian and 0.21 km for the Burdigalian–Serravallian (Figure 7a). The unit displays an overall uniform thickness within the extensional and contractional zones, but thickens within an intraslope basin, located seaward of the thrust fault (labelled T in Figure 4d). The late Eocene–Serravallian Unit locally thins at the top of bathymetric highs formed by thrust/shale-cored anticlines (e.g. the thrust faults labelled T, U in Figure 4d). The late Eocene–Serravallian Unit is locally truncated within the IFTB by the Tortonian surface (Figure 4e).

Interpretation

The overall uniform thickness of the late Eocene–Serravallian Unit across the normal faults (labelled P–S and I–O in Figures 3–5) suggests that the modern offshore western Niger Delta's extensional zone was not active during the late Eocene and the Serravallian. This interpretation supports the location of the 'Oligocene-Tortonian' extensional zone within fault-bounded accommodation in the present-day onshore (see Wiener et al., 2010; Figure 1b). However, the seaward increase in thickness of the late Eocene–Serravallian Unit within the hanging wall of the thrust fault (labelled T in Figure 4d) could be interpreted as growth strata associated with the activity of the thrust fault. Although this observation coupled with the corresponding thinning of the late Eocene–Serravallian Unit at the crest of thrusts/shale-cored anticlines (Figure 4d) further supports that the underlying thrusts/ duplexes were active during the deposition of the unit, similar stratigraphic architecture has also been linked to differential compaction by other authors (e.g. Maloney et al., 2010). Similarly, the undulating geometry of the late Eocene, Burdigalian and Serravallian surfaces within intraslope basins (Figures 3, 4a,b,d,e and 5a,b) supports differential compaction or the activity of the underlying duplexes during the late Eocene–Serravallian. The abrupt truncation of the Burdigalian surface by the Serravallian surface in the IFTB (Figure 4e) suggests that the activity of the underlying duplexes, caused local instability,

allowing erosion/remobilisation at the crest of thrust/shale-cored anticlines, associated with the thrust faults (labelled V and W in Figure 4e).

4.1.3 The Serravallian–Tortonian Unit (12.5–9.5 Ma)

Description

The Serravallian–Tortonian Unit is bounded at the base by the Serravallian surface described above and at the top by the Tortonian surface (highlighted in light green in Figures 3–6). The Tortonian surface generally truncates seismic reflectors at the crest of thrust/shale-cored anticlines within the IFTB (Figure 4e). Estimated average thickness of the Serravallian–Tortonian Unit is 0.24 km (Figure 7a). The unit displays an overall constant thickness within the outer-fold-thrust belt (OFTB), but slightly thickens on the hanging walls of the normal faults (labelled S in Figures 3 and 4c, and I, J in Figure 5a,b). The Serravallian–Tortonian Unit generally thins above thrusts/ shale-cored anticlines within the translational zone and inner-fold-thrust belt (IFTB), but thickens within the adjacent intraslope basins (e.g. Figure 4d,e). Along the 500km, delta-wide strike line located on the continental shelf (Figure 1b), the Serravallian–Tortonian Unit shows an overall constant thickness in the ENDL (Figure 6c,d). The Serravallian–Tortonian Unit increases in thickness to the WNDL, and on the hanging walls of listric normal faults above the Chain Fracture Zone (Figure 6e).

Interpretation

The truncation of seismic reflectors (e.g. the Burdigalian and Serravallian) by the Tortonian surface within the IFTB (Figure 4e) suggests that the activity of the underlying duplexes caused instability, allowing erosion at the crest of thrust/shale-cored structures (e.g. Figure 4e). The local thickening of the Serravallian–Tortonian Unit on the hanging walls of the normal faults (labelled S in Figures 3 and 4c, and I and J, in Figure 5) is interpreted as growth strata, synchronous with the deposition of the unit. Similarly, the overall thickening of the Serravallian– Tortonian Unit within intraslope basins in the translational zone and the corresponding thinning at the top of thrust/ shale-cored anticlines (Figure 4d,e) are interpreted as recording syn-depositional activity of the underlying thrusts/ mobile shales. The along-strike variation in thickness of the unit, with an overall thickening from ENDL to WNDL, is interpreted as recording differential subsidence/compaction, and changes in location of sediment input to the delta (see also Jermannaud et al., 2010; Rouby et al., 2011; Figure 6b–e).

4.1.4. The Tortonian–early Pliocene Unit (9.5–4.9 Ma)

Description

The Tortonian–early Pliocene Unit is bounded at the base by the Tortonian surface described above, and at the top by the early Pliocene surface (highlighted in red in Figures 3–6). The Tortonian and early Pliocene reflectors locally display undulating, concave-upward geometry, marked by abrupt truncations of the underlying reflectors notably at the crest of thrust/shale-cored anticline within the extensional and translational zones, as well as the IFTB (Figures 3 and 4d–e). The Tortonian–early Pliocene Unit reaches an average thickness of 0.25 km (Figure 7a). It displays a lateral variation in thickness with local thickening on the hanging walls of the normal faults (labelled Q and S in Figures 3 and 4c, and I, J in Figure 5b). The Tortonian–early Pliocene Unit generally thins above thrust/shale-cored anticlines (Figures 3 and 4d–f), but thickens within the adjacent intraslope basins (e.g. Figure 4d,e). Along the delta-wide seismic line on the continental shelf (Figure 1a), the Tortonian–early Pliocene displays a lateral variation in thickness with an overall increase from the eastern to western Niger Delta lobe (Figure 6c–e).

Interpretation

The local truncations of reflectors below the Tortonian and early Pliocene surfaces suggest their erosional character, linked to the activity of the underlying thrusts (labelled T in Figure 4d, V, W in Figure 4e, and X in Figure 4f). The reflectors truncated at the early Pliocene surface, seaward of the bathymetric high (labelled BH in Figure 5b), is also linked to the activity of the underlying thrust. The overall thickening of the Tortonian–early Pliocene Unit across the hanging walls of the normal faults (labelled Q, S in Figures 3 and 4c, and I, J in Figure 5b) is interpreted as growth strata. The along strike variation in thickness of the Tortonian–early Pliocene Unit, with an overall thickening from ENDL to WNDL, is interpreted as recording differential subsidence probably in response to changes in sediment loading (see also Jermannaud et al., 2010; Rouby et al., 2011; Figure 6b–e). The general increase in thickness of the Tortonian–early Pliocene Unit, within intraslope basins, and the concomitant thinning at the crest of thrust/shale-cored anticlines (Figures 4d,f and 5b), are interpreted as syn-depositional deformation (see also Maloney et al., 2010). The relatively smooth geometry of the Tortonian–early Pliocene surfaces within the intraslope basin, seaward of the thrust fault (labelled T, U in Figure 4d), suggests that the underlying duplexes were not active during the deposition of the unit. However, the undulating geometry of the Tortonian–early Pliocene surfaces further west of the study area (Figures

3 and 5b) suggests activity of the underlying thrusts. The erosional character of the early Pliocene surface in the extensional zone (Figures 3 and 4c), translational zone and IFTB (Figures 3 and 4d,e) suggests the possible development of the surface during a relative sea-level fall and increase in sediment supply in the early Pliocene (see also Chima et al., 2019, 2020).

4.1.5. The early Pliocene–early Pleistocene Unit (4.9–5.0 to ca. 2.6 Ma)

Description

The early Pliocene–early Pleistocene Unit is bounded at the base and top by the seismic reflectors marked in red and dark yellow respectively in Figures 3–6. The early Pliocene and early Pleistocene surfaces locally truncate seismic reflectors within the extensional and translational zones, as well as IFTB and OFTB (e.g. Figures 3, 4c–f and 5b). The early Pliocene–early Pleistocene Unit reaches an average thickness of 0.23 km (Figure 7a). It is generally thicker on the hanging walls of the normal faults (labelled Q, P, S, in that order), on the shelf than in intraslope basins in the translational zone (Figures 3, 4b–d and 5b). The early Pliocene–early Pleistocene Unit thickens within intraslope basins in the translational zone and IFTB, but thins above shale/thrust-cored anticlines, down to the OFTB, where it onlaps a basement high (labelled BH in Figures 3, 4b–f and 5b). Within the early Pliocene–early Pleistocene Unit, seaward-inclined linear scars (hashed white lines in Figure 4d,e) are locally present at the top of thrust/shale-cored anticlines that are flanked by mass-transport deposits (MTDs) in the translational zone. On the delta-wide strike line on the continental shelf (Figure 1a), the early Pliocene–early Pleistocene Unit shows a lateral variation in thickness with an overall thinning to the eastern and western edges of the delta. The early Pliocene–early Pleistocene Unit thickens towards the central part of the delta (Figure 6b–e). The observed lateral variation in thickness along the delta-wide strike line is partially controlled by the alignment of the line with growth faults in the eastern, central and western part of the delta (Figure 1a).

Interpretation

The truncations of reflectors by the early Pliocene surface on the continental shelf and slope (e.g. Figures 3 and 4c–e) suggests its erosional character, probably developed during a sea-level fall in the early Pliocene (see also Chima et al., 2020). The presence of seaward-dipping scars (interpreted as headwall scars) at the crest of thrust/shale-cored anticlines (Figure 4d,e) suggests the role of thrusting in triggering mass wasting. This interpretation is supported by the presence of MTDs within the

adjacent intraslope basins (Figure 4d,e). The general truncation of reflectors by the early Pliocene surface at the crest of thrust/shalecored anticlines (e.g. Figures 3, 4d–f and 5b) suggests syndepositional activity of the structures. This interpretation is supported by the overall thinning of the early Pliocene–early Pleistocene Unit above thrust/shale-cored structures, and the concomitant thickening within intraslope basins (e.g. Figures 3, 4d–f and 5b). The general thickening of the early Pliocene–early Pleistocene Unit on the continental shelf and the upper slope (Figures 3, 4b–d and 5b) is interpreted to record syn-depositional deformation during the deposition of the unit. The onlapping of early Pliocene–early Pleistocene Unit on bathymetric highs in the translational and contractional zones (Figures 3, 4d–f and 5b) indicates that gravity-driven deformation was accommodated down-dip by shortening/folding.

4.1.6. The early Pleistocene–present (ca. 2.6–0 Ma)

Description

The early Pleistocene–present Unit is bounded at the base by the early Pleistocene surface and capped by the seafloor (Figures 3–6). The early Pleistocene–present Unit is marked in the middle by a downlap surface (yellow reflector in Figures 3–6). This downlap surface corresponds to the erosional surface, dated on the continental slope as the middle Pleistocene transition (0.8–1.0 Ma) (see figs. 3 and 10 in Chima et al., 2020). The early Pleistocene surface locally truncates the upper part of the Pliocene sediments in the extensional and translational zones, and OFTB (Figures 3 and 4e,f). The early Pleistocene–present Unit locally displays seaward-inclined scarps at the crest of thrust/shale-cored anticlines, which are flanked by MTDs in the adjacent intraslope basins (Figure 4d,e). The unit reaches a highest average thickness of 0.5 km (Figure 7a). The early Pleistocene–present Unit reaches maximum thickness on the continental shelf and upper slope, but gradually thins seaward to the OFTB, where it onlaps bathymetric highs (Figures 3, 4b–f and 5b). Along the delta-wide strike line displayed in Figure 6a,b, the early Pleistocene–present Unit generally decreases in thickness from the eastern to the western Niger Delta lobe (Figure 6a–e).

Interpretation

The truncation of seismic reflectors on the continental shelf by the early Pleistocene surface (e.g. Figure 3), suggests its erosional character. This interpretation is supported by the erosional truncations of reflectors below the early Pleistocene surface in the IFTB and OFTB (Figure 4e,f). The presence of

headwall scarps at the crest of thrust/ shale-cored anticlines (Figure 4d,e), further supports the role of thrusting at steepening the slope and increasing its instability, allowing mass wasting on the continental slope. The truncation of reflectors at the crest of thrust/ shale-cored anticlines (e.g. Figures 3 and 4d–f) suggests the activity of the structures during the Pleistocene. The overall thickening of the early Pleistocene–present Unit within the hanging walls of normal faults in the extensional and translational zones is interpreted to record syn-depositional deformation (Figures 3–6). However, the overall thinning/onlapping of the unit within the deep basin (Figures 3–5) suggests that gravity collapse of the continental shelf and upper slope facilitated the creation of accommodation for sediment sequestration. The increase in thickness of the early Pleistocene–present Unit to the ENDL (Figure 6a,b) suggests an overall increase flexural subsidence, linked to increase in sediment loading and/or gravity collapse of the eastern Niger Delta continental shelf.

4.2. Sedimentation rate

Estimated average sedimentation rates on key 2D seismic lines in the offshore WNDL (Figure 7b) show relatively low depositional rates from late Eocene to Burdigalian. Average sedimentation rates range between 0.01 and 0.03 km/Myr, respectively, during the late Eocene–Serravallian, to 0.08 and 0.16 km/Myr over the Serravallian–Tortonian. Sedimentation rates, thus, display at least a two-fold increase from the Burdigalian to the Tortonian. They gradually decrease by one third from the Tortonian to early Pliocene, and finally doubled from the early Pliocene to present (Figure 7b), reaching respective peaks of 0.20 and 0.25 km/Myr at present-day.

5. Discussion

Regional depth-penetrating 2D seismic reflection data and calibration with well information allow us to discuss the tectono-stratigraphic evolution of the offshore western Niger Delta. We focus on the control of delta dynamics and paleo-topography on gravity-driven deformation of the delta from the Cretaceous to present. We also compare the stratigraphic architecture of the offshore WNDL with the ENDL over the Pliocene and Pleistocene.

5.1. Tectono-stratigraphic evolution of the offshore WNDL from the Cretaceous to present

The overall thinning of the late Eocene–Serravallian at the crest of the thrust/shale-cored anticline, and its thickening within the intraslope basin, seaward of the thrust fault (labelled T in Figure 4d),

suggest syn-depositional deformation. This interpretation is supported by the undulating geometry of the late Eocene, Burdigalian and the Serravallian surfaces, interpreted as recording the activity of the underlying duplexes (Figures 3, 4b,d and 5b). Magmatic upwelling and catchment reorganisation around ca. 34–29 Ma, as well as an increase in sediment supply in the offshore Niger Delta, reported by Chardon et al. (2016) and Grimaud et al. (2017), is thought to have triggered deformation of the late Eocene–Serravallian Unit. However, the overall uniform thickness of the late Eocene–Serravallian Unit within the extensional zone (Figures 3–5) suggests that the depocenter was probably confined in fault-bounded accommodation in the present-day onshore (Figure 1b). This interpretation agrees with previous studies of the ENDL, where deposition is reported to have been focused in the current onshore part (the ‘Oligocene-Tortonian extensional zone’ [see Bilotti et al., 2005; Wiener et al., 2010]). During the Serravallian and the Tortonian, the presence of growth strata on the hanging walls of the normal faults (labelled S in Figures 3 and 4c; I and J in Figure 5a,b) suggests the onset of deformation within the currently active extensional zone. The overall thinning of the Serravallian–Tortonian Unit at the crest of thrust/mobile shale-cored anticlines, and its concomitant thickening within intraslope basins (Figures 3–5), suggest that deformation within the extensional zone was accommodated by shortening/folding within the translational and contractional zones. The coupling between extensional deformation and shortening suggests the onset of sediment bypass from depocenter fill in the ‘Oligocene-Tortonian extensional zone’ (the present-day onshore; Figure 1b).

During the Tortonian–early Pliocene, the presence of growth strata from the extensional to contractional zones (e.g. Figures 3, 4c–f and 5b) is interpreted to record regional, syn-depositional deformation. This regional deformation could be linked to the onset of seaward migration of the ‘Oligocene-Tortonian extensional zone’ from the present-day onshore to the modern continental shelf (see Bilotti et al., 2005; Wiener et al., 2010; Figure 1b). In the ENDL, the migration of the ‘Oligocene-Tortonian extensional zone’ from the onshore to its present-day position (Figure 1b) was linked to an overall increase in sedimentation during the Tortonian (see Bilotti et al., 2005; Wiener et al., 2010). The relatively low sedimentation rate over the Tortonian–early Pliocene (Figure 1b) could be linked to uncertainties in biostratigraphic dating, seismic interpretation or velocity modelling, used in time-to-depth conversion.

The general thickening of the early Pliocene–early Pleistocene Unit within the extensional zone (e.g. Figures 3, 4b,c, 5b and 6d,e) suggests an overall increase in deposition on the offshore western Niger Delta's continental shelf. This agrees with the incisional character of the early Pliocene surface (e.g. Figures 3 and 4c–e). The thinning/onlapping of the early Pliocene–early Pleistocene Unit at the crest of thrust/shale-cored anticlines and thickening of the unit within adjacent intraslope basins (e.g. Figures 4d–e and 5b) suggests that extensional deformation was accommodated by shortening in the deep basin. Sediment loading on the continental shelf, aided by the presence of a structural barrier,

formed by thrust/shale-cored anticline (e.g. Figure 4), are inferred to have facilitated gravity spreading (see review in Morley et al., 2011). Gravity spreading is also inferred to have been triggered by the presence of a seaward dipping bathymetric surface (Peel, 2014; Rowan et al., 2004; SchultzEla, 2001; Figures 3, 4b and 5b). The onlapping of the early Pliocene–early Pleistocene Unit on a relief associated with the imbricated thrust (labelled Z in Figure 4f) supports the initiation of the OTFB during the early Pliocene (see Wiener et al., 2010).

The remarkable increase in sediment thickness over the early Pleistocene–present (Figures 3–6) continued to drive gravity collapse/increase in accommodation, and gravity spreading of the offshore WNDL. The onlapping of the early Pleistocene–present Unit on a bathymetric relief on the modern seafloor (Figure 4f) indicates that the OFTB of the offshore WNDL was active in the Pleistocene, and may still be active. We propose a five-stage schematic illustration of the tectono-stratigraphic evolution of the offshore WNDL from the late Cretaceous to present (Figures 8 and 9). (a) Development of duplexes within the upper detachment unit; (b) initiation of gravity-driven deformation within the currently active extensional and translational zones; (c) coupling of deformation between the extensional, translational and contractional zones, and inferred migration of the ‘Oligocene-Tortonian extensional zone’ from the present-day onshore to the present-day continental shelf; (d) acceleration of gravity collapse of the continental shelf, and initiation of the OFTB; (e) intensification of gravity collapse and deformation at the leading front of the OFTB.

5.2. Controls of paleo-topography and delta dynamics on gravity-driven deformation of the offshore WNDL

The bathymetric highs formed by the Charcot and Chain Fracture Zones (Figures 1a,b and 6a,b,d,e) acted as transform faults during the opening of the equatorial Atlantic in the middle Aptian (Briggs et al., 2009; Lehner & de Ruiter, 1997). Although these relict transform faults are known to have been inactive in the Santonian (Briggs et al., 2009; Lehner & de Ruiter, 1997), their relict topographies control the architecture of younger post-rift sediments. The relict Charcot and Chain Fracture Zones have been identified to have exerted a long-term depositional control (loading/differential compaction) on the architecture of Ghana and Ivory Coast in the west African margin (de Matos, 2000). The Chain Fracture Zones generally act as transfer zone for sediment partitioning to the deep basin (Krueger & Grant, 2011).

In this study, the general thinning of the late Cretaceous–Serravallian Unit at the crest of the relict Charcot and Chain Fracture Zones (Figure 6a,b,d,e) suggests that the presence of these paleo-topographies exerted depositional control on the geometry of the unit. The thinning trend above these

paleo-topographies, and concomitant thickening on the flanks, support their role in buttressing or localising strain (see also Briggs et al., 2009; Davies et al., 2005; Figures 1b and 6a–e). This interpretation is supported by the presence of listric, synthetic and antithetic faults, above the Charcot and Chain Fracture Zones (Figure 6d,e). Although the Chain and Charcot Fracture Zones are generally interpreted as presently inactive, the concentration of listric and synthetic normal faults above these structures supports their role in strain localisation in addition to gravity-driven deformation and mechanical compaction. The observed higher sediment thickness at the flanks of the relict transform faults (Figure 6a–f) has the potential of increasing regional overpressure within the detachment (Figures 3–5). Also, differential subsidence on both sides of the relict transform faults is responsible for the segmentation of gravity-driven deformation in the eastern and western Niger Delta lobes (see Wu et al., 2015). Although no evidence of re-activation of these paleo-transforms faults was observed in our data, their long-term control is visible on the architecture of the offshore WNDL (Figure 6a–f).

5.3. Implication of sedimentation rates on the evolution of the offshore WNDL

In this study, the estimated average sedimentation rates on the offshore WNDL display similar trend with Grimaud et al. (2017), with a relatively low depositional rates from the late Eocene to Burdigalian, and late Eocene to Langhian respectively (Figure 7b). The magmatic upwelling of the Hoggar Mountain and re-organisation of the Niger catchment around ca. 34–29 Ma are reported to have initiated an increase in sedimentation rate on the offshore Niger Delta (Chardon et al., 2016; Grimaud et al., 2017). However, the observed low sedimentation rate over the late Eocene–Burdigalian could be linked to (a) sediment trapping within the ‘Oligocene-Tortonian extensional zone’ (the present-day onshore; Figure 1b) or (b) compaction/porosity loss due to increase in burial depth. The overall increase in average sedimentation rate from the Burdigalian to Tortonian (Figure 7b) is consistent with Grimaud et al. (2017). The increase in sediment supply is probably linked to a combination of sustained erosion of the Hoggar region (see Grimaud et al., 2017), and/or intensification of sediment cannibalisation on the continental shelf as documented in other continental margins (see Anka et al., 2009; Grimaud et al., 2017; Séranne & Nzé Abeigne, 1999). The incision of the Niger Delta's continental shelf during the Miocene was first reported by the presence of clay-filled, Opuama channel complex (see Doust & Omatsola, 1990; Figure 1d). Grimaud et al. (2017), reported a general high sedimentation rate over the Tortonian–early Pliocene (Figure 7b). However, the relatively low average sedimentation rate that we estimated during the Tortonian–early Pliocene (Figure 7b) could be linked to (a) sediment trapping within the Niger catchment and/ or (b) sediment routing from west to east (Figure 1b). The slight decrease in average sedimentation rate in the offshore WNDL during the Tortonian (Figure 7b) differs from the overall increase reported in the ENDL by Wiener et al. (2010) and Jolly et al. (2016). Like

Rouby et al. (2011) and Grimaud et al. (2017), our estimated average sedimentation over the Pliocene–Pleistocene displays a (more than) two-fold increase (Figure 7b). Earlier studies by Wiener et al. (2010), Robin et al. (2011), Rouby et al. (2011), Chardon et al. (2016) and Grimaud et al. (2017) linked the increase in sediment supply to the offshore Niger Delta over the Pliocene–Pleistocene to climatically forced precipitation. Chima et al. (2020) suggested that glacio-eustatic sea-level oscillation of 400-kyr eccentricity, and intensification of West African Tropical Monsoon, could explain the general increase in sedimentation rate on the offshore WNDL during the Pliocene–Pleistocene.

Contrary to Rouby et al. (2011) and Grimaud et al. (2017), who documented a general decrease in sedimentation rate from the Pleistocene to present, our results show an overall increase in sedimentation rates (Figure 7b). Although Grimaud et al. (2017) linked their estimated low sedimentation rate in the offshore WNDL during the Pleistocene to sediment trapping within the Niger catchment, their lack of data in the distal offshore could also explain their low interpreted depositional rates. Rouby et al. (2011) linked their observed reduction in sedimentation rate in the offshore ENDL from the Pleistocene to present to aridification of West Africa or a possible transfer of sediment flux from the ENDL to WNDL. The high sedimentation rates observed in this study from the Pleistocene to present are consistent with sediment budgets in other worldwide passive continental margins, for example, the offshore Alaska (Gulick et al., 2015) and the Alpine region (Hay, 1998; Leroux et al., 2017; Molnar & England, 1990; Willett, 2010). In these regions, the increase in sedimentation rate during most of the Pleistocene (Figure 7b) is attributed to glacio-eustatic sea-level changes of 100-kyr eccentricity, and intensification of the West African Tropical Monsoon at the middle Pleistocene Transition (MPT, ca. 0.8–1.0 Ma) (see also Chima et al., 2020).

5.4. The Pliocene and Pleistocene stratigraphic architecture; eastern versus western Niger Delta lobes

Comparison of regional dip lines from the eastern and western Niger Delta lobes over the Pliocene and the Pleistocene reveals that variation in structural patterns in these regions controlled their stratigraphic architecture (Figure 10a,b). The ENDL displays an overall higher slope angle compared to the WNDL (Figure 10a,b). The higher shelf-slope angle of the ENDL compared to the WNDL could be linked to the presence of seamount or buried volcanoes (e.g. de Matos, 2000; Mourgues et al., 2009). This interpretation is supported by the proximity of the seismic line (Figure 10a) to the Fernando Po Fracture Zone (Figure 1a,b).

Although the continental shelves of the ENDL and WNDL are characterised by seaward-and landwarddipping normal faults, they display overall progradation during the late Pliocene and the early

Pliocene respectively (Figure 10a,b). The presence of well-developed counter-regional normal faults at the shelf-slope break of the ENDL favoured aggradation and sediment sequestration on the continental shelf and slope regions from the Pleistocene to present (Figure 10a). However, the dominance of well-developed seaward-dipping normal faults in the WNDL favoured an overall progradation and sediment bypass to the deep basin from the Pleistocene to present (Figure 10b). We propose two possible explanations for the dominance of counter-regional normal faults on the continental shelf of the ENDL; (a) the relief formed by the Fernando Po Fracture Zone or buried volcanoes, thereby localising strain and (b) the presence of buried thrust faults (see also Sapin et al., 2012).

We lack sufficient seismic and well data for complete source-to-sink mapping and estimation of sedimentation rates for a robust quantitative comparison between ENDL and WNDL. However, the observed geometries (Figure 10a,b) clearly demonstrate that differences in gravity-driven deformation in these regions significantly controlled their evolution in a similar way during the Pliocene but differently during the Pleistocene.

6. Conclusions

1. Limited sedimentary wedge deformation within the extensional and translational zones, offshore WNDL, from the late Eocene to Serravallian, suggests that the 'Oligocene-Tortonian extensional zone' is buried under the present-day onshore area. Regional distribution of deformation from the extensional zone to the transitional detachment fold-belt during the Tortonian suggests seaward progradation.
2. An overall increase in sedimentation on the continental shelf, offshore WNDL since the Serravallian, characterised by deformation within the extensional and translational zones, is thought to have triggered gravity-driven deformation. The increase in sedimentation in the Pliocene and Pleistocene, differential subsidence of the continental shelf and slope and the presence of seawarddipping bathymetry aided the acceleration of gravity spreading. The increase in sedimentation rates during the Pliocene–Pleistocene, coupled with the presence of bathymetric relief on the modern seafloor, at the leading front of the contractional zone, supports the development of the present-day outer-fold-thrust belt in the Pliocene.
3. Paleo-topographies formed by the Charcot and Chain Fracture Zones, which developed during the opening of the equatorial Atlantic, exerted depositional control on the stratigraphic architecture of the offshore WNDL from the Cretaceous to Serravallian. High sedimentation rates and differential subsidence across the relict Chain and Charcot Fracture Zones segmented gravity-driven deformation in the eastern and western Niger Delta lobes.

4. The eastern and western Niger Delta lobes display an overall progradation and sediment bypass to the deep basin during the Pliocene. However, overall WNDL progradation continued during the Pleistocene, while the ENDL retrograded due to sediment sequestration on the continental shelf and upper slope. The ENDL and WNDL display complex spatial and temporal variations in gravity-driven deformation, and sediment partitioning, during the Pliocene and the Pleistocene. Hence, more regional seismic and well data are needed for a more complete source-to-sink analysis of the systems.
5. We propose a five-stage evolution of the offshore WNDL from the late Cretaceous to present.

Acknowledgements

The Federal Republic of Nigeria sponsored the PhD of Kelvin Ikenna Chima under the auspices of the Petroleum Technology Development Fund (PTDF) Scholarship Programme. We are grateful to Shell Nigeria not only for providing the data, which we used in this study but also for the permission to publish it. PTDF and Schlumberger provided the computer workstation and Petrel(TM) software, respectively, used in data analysis and interpretation. The corresponding author would like to thank immensely the management and staff of Alex Ekwueme Federal University, Ndufu-Alike Ikwo, Ebonyi State Nigeria for their support and encouragement throughout this research. This study was carried out at the Institut des Sciences de la Terre (ISTeP), Paris. Special thanks to Olusegun Obilaja, Adekemi Afolayan, Babatope Atitebi, Richard Streatfield and Timi Tralagba (Shell Nigeria) for their invaluable support with data. Insightful discussion with Daniel Praeg (GeoAzur France) helped in improving the quality of this paper. We thank the editor-in-chief, Atle Rotevatn, for granting us sufficient time to revise this paper. David M. Hodgson, Danielle Howlett and an anonymous reviewer are specially thanked for their constructive comments and suggestions.

References

- Adeogba, A. A., McHargue, T. R., & Graham, S. A. (2005). Transient fan architecture and depositional controls from near-surface 3D seismic data, Niger Delta continental slope. *AAPG Bulletin*, 89, 627–643. <https://doi.org/10.1306/11200404025>
- Anka, Z., Séranne, M., Lopez, M., Scheck-Wenderoth, M., & Savoye, B. (2009). The long-term evolution of the Congo deep-sea fan: A basin-wide view of the interaction between a giant submarine fan and a mature passive margin (ZaiAngo project). *Tectonophysics*, 470, 42–56. <https://doi.org/10.1016/j.tecto.2008.04.009>
- Avbovbo, A. A. (1978). Tertiary lithostratigraphy of the Niger Delta. *AAPG Bulletin*, 62, 295–300.

- Bakare, O., Hurley, N., & McHargue, T. (2007). Effect of growing structures on stratigraphic evolution, channel architecture, and submarine fan distribution, Niger Delta, West Africa. AAPG Conference Proceedings, California.
- Bellingham, P., Connors, C., Haworth, R., Barbara, R., & Danforth, A.L. (2014). The deep-water Niger delta: An underexplored world class petroleum province. *Petroleum Geoscience Magazine*, 11, 1–9.
- Bilotti, F. D., Shaw, J. H., Cupich, R. M., & Lakings, R. M. (2005). Detachment fold, Niger Delta. In J. H. Shaw, C. Connors, & J. Suppe (Eds.), *Seismic interpretation of contractional fault related folds: AAPG studies in geology* (Vol. 53, pp. 103–104). American Association of Petroleum Geologists (AAPG).
- Briggs, S. E., Cartwright, J., & Davies, R. (2009). Crustal structure of the deepwater west Niger Delta passive margin from the interpretation of seismic reflection data. *Marine and Petroleum Geology*, 26, 936–950. <https://doi.org/10.1016/j.marpetgeo.2008.07.003>
- Briggs, S. E., Davies, R. J., Cartwright, J. A., & Morgan, R. (2006). Multiple detachment levels and their control on fold styles in the compressional domain of the deep-water west Niger Delta. *Basin Research*, 18, 435–450. <https://doi.org/10.1111/j.1365-2117.2006.00300.x>
- Chardon, D., Grimaud, J.-L., Rouby, D., Beauvais, A., & Christophoul, F. (2016). Stabilization of large drainage basins over geological time scales: Cenozoic West Africa, hot spot swell growth, and the Niger River: Hot spot swell growth and Niger River. *Geochemistry, Geophysics, Geosystems*, 17, 1164–1181. <https://doi.org/10.1002/2015GC006169>
- Chima, K. I., Do Couto, D., Leroux, E., Gardin, S., Hoggmasacall, N., Rabineau, M., Granjean, D., & Gorini, C. (2019). Seismic stratigraphy and depositional architecture of Neogene intraslope basins, offshore western Niger Delta. *Marine and Petroleum Geology*, 109, 449–468. <https://doi.org/10.1016/j.marpetgeo.2019.06.030>
- Chima, K. I., Gorini, C., Rabineau, M., Granjean, D., Do Couto, D., Leroux, E., & Hoggmascall, N. (2020). Pliocene and Pleistocene stratigraphic evolution of the western Niger Delta intraslope basins: A record of glacio-eustatic sea-level and basin tectonic forcings. *Global and Planetary Change*, 195, 103355. <https://doi.org/10.1016/j.gloplacha.2020.103355>
- Cobbold, P. R., Clark, B. J., & Løseth, H. (2009). Structural consequences of fluid overpressure and seepage forces in the outer thrust belt of the Niger Delta. *EAGE*, 15, 3–15.
- Cobbold, P. R., Mourgues, R., & Boyd, K. (2004). Mechanism of thin-skinned detachment in the Amazon Fan: Assessing the importance of fluid overpressure and hydrocarbon generation. *Marine and Petroleum Geology*, 21, 1013–1025. <https://doi.org/10.1016/j.marpetgeo.2004.05.003>
- Cohen, H. A., & McClay, K. (1996). Sedimentation and shale tectonics of the northwestern Niger Delta front. *Marine and Petroleum Geology*, 13, 313–328. [https://doi.org/10.1016/02648172\(95\)00067-4](https://doi.org/10.1016/02648172(95)00067-4)

- Corredor, F., Shaw, J. H., & Bilotti, F. (2005). Structural styles in the deep-water fold and thrust belts of the Niger Delta. *AAPG Bulletin*, 89, 753–780. <https://doi.org/10.1306/02170504074>
- Damuth, J. E. (1994). Neogene gravity tectonics and depositional processes on the deep Niger Delta continental margin. *Marine and Petroleum Geology*, 11, 320–346. [https://doi.org/10.1016/0264-8172\(94\)90053-1](https://doi.org/10.1016/0264-8172(94)90053-1)
- Davies, R. J., MacLeod, C. J., Morgan, R., & Briggs, S. E. (2005). Termination of a fossil continent-ocean fracture zone imaged with three-dimensional seismic data: The Chain Fracture Zone, eastern equatorial Atlantic. *Geology*, 33(8), 641–644. <https://doi.org/10.1130/G21530AR.1>
- de Matos, R. M. D. (2000). Tectonic evolution of the equatorial Atlantic. *Geophysical Monograph*, 115, 331–354.
- Dejong, K. A., & Scholten, R. (1973). *Gravity and tectonics* (p. 502). John Wiley.
- Doust, H., & Omatsola, E. (1990). Niger Delta. In J. D. Edwards & P.A. Santogrossi (Eds.), *Divergent passive margin basins* (Vol. 48, pp. 239–248). American Association of Petroleum Geologists (AAPG) Bulletin.
- Evamy, B. D., Haremboure, J., Kammerling, R., Knaap, W. A., Molloy, F. A., & Rowlands, P. H. (1978). Hydrocarbon habitat of Tertiary Niger Delta. *AAPG Bulletin*, 62, 1–39.
- Gibbard, P. L., Head, M. J., & Walker, M. J. (2014). Subcommittee on stratigraphy Formal ratification of the Quaternary System/ Period and Pleistocene Series/Epoch with a base at 2.5 Ma. *Quaternary Science*, 245, 96–102.
- Grimaud, J.-L., Rouby, D., Chardon, D., & Beauvais, A. (2017). Cenozoic sediment budget of West Africa and the Niger delta. *Basin Research*, 30(2), 169–186.
- Gulick, S. P. S., Jaeger, J. M., Mix, A. C., Asahi, H., Bahlburg, H., Belanger, C. L., Berbel, G. B. B., Childress, L., Cowan, E., Drab, L., Forwick, M., Fukumura, A., Ge, S., Gupta, S., Kioka, A., Konno, S., LeVay, L. J., März, C., Matsuzaki, K. M., ... Swartz, J. M. (2015). Mid-Pleistocene climate transition drives net mass loss from rapidly uplifting St. Elias Mountains, Alaska. *Proceedings of the National Academy of Sciences of the United States of America*, 112, 15042–15047. <https://doi.org/10.1073/pnas.1512549112>
- Haack, R. C., Sundararaman, P., Diedjonmahor, J. O., Hongbin, X., Gant, N. J., May, E. D., & Kelsch, K. (2000). Niger Delta petroleum systems, Nigeria. In M. R. Mello, & B. J. Katz (Eds.), *Petroleum systems of South Atlantic margins* (Vol. 73, pp. 213–231). American Association of Petroleum Geologists (AAPG) Memoir.
- Hay, W. W. (1998). Detrital sediment fluxes from continents to oceans. *Chemical Geology*, 145, 287–323. [https://doi.org/10.1016/S0009-2541\(97\)00149-6](https://doi.org/10.1016/S0009-2541(97)00149-6)
- Jermannaud, P., Rouby, D., Robin, C., Nalpas, T., Guillocheau, F., & Raillard, S. (2010). Plio-Pleistocene sequence stratigraphic architecture of the eastern Niger Delta: A record of eustasy and

- aridification of Africa. *Marine and Petroleum Geology*, 27, 810–821.
<https://doi.org/10.1016/j.marpetgeo.2009.12.005>
- Jolly, B. A., Lonergan, L., & Whittaker, A. C. (2016). Growth history of fault-related folds and interaction with seabed channels in the toe-thrust region of the deep-water Niger Delta. *Marine and Petroleum Geology*, 70, 58–76. <https://doi.org/10.1016/j.marpetgeo.2015.11.003>
- Krueger, S. W., & Grant, N. T. (2011). The growth history of the toe thrusts of the Niger Delta and the role of pore pressure. In K. R. McClay, J. H. Shaw, & J. Suppe (Eds.), *Thrust fault-related folding* (Vol. 94, pp. 357–390). American Association of Petroleum Geologists (AAPG) Memoir.
- Lehner, P., & de Ruiter, P. A. C. (1997). Structural history of Atlantic margin of Africa. *AAPG Bulletin*, 61(7), 961–981.
- Leroux, E., Rabineau, M., Aslanian, D., Gorini, C., Molliex, S., Bache, F., Robin, C., Droz, L., Moulin, M., Poort, J., Rubino, J.-L., & Suc, J. P. (2017). High-resolution evolution of terrigenous sediment yields in the Provence Basin during the last 6 Ma: Relation with climate and tectonics. *Basin Research*, 29(9), 305–339.
- Maloney, D., Davies, R., Imber, J., Higgins, S., & King, S. (2010). New insights into deformation mechanisms in the gravitationally driven Niger Delta deep-water fold and thrust belt. *AAPG Bulletin*, 94(9), 1401–1424. <https://doi.org/10.1306/01051009080>
- Mitchum, R. M., & Vail, P. R. (1977). Seismic stratigraphy and global changes of sea level, Part 7: Seismic stratigraphic interpretation procedure. In C. E. Payton (Ed.), *Seismic stratigraphy: Applications to hydrocarbon exploration* (Vol. 26, pp. 135–143). American Association of Petroleum Geologists (AAPG) Memoir.
- Molnar, P., & England, P. (1990). Late Cenozoic uplift of mountain and global climate change: Chicken or egg? *Nature*, 343, 29–34.
- Morgan, R. (2004). Structural controls on the positioning of submarine channels on the lower slopes of the Niger Delta. In R. J. Davies, J. Cartwright, S. A. Stewart, J. R. Underhill, & M. Lappin (Eds.), *3D seismic technology: Application to the exploration of sedimentary basins* (Vol. 29, pp. 45–51). Geological Society of London Memoir.
- Morley, C. K., King, R., Hillis, R., Tingay, M., & Backe, G. (2011). Deep water fold and thrust belt classification, tectonics, structure and hydrocarbon prospectivity. *Earth Science Reviews* 104, 41-94.
- Mourgues, R., Lecomte, E., Vendeville, B., & Raillard, S. (2009). An experimental investigation of gravity-driven shale tectonics in progradational delta. *Tectonics*, 474, 643–656.
- Peel, F. J. (2014). The engines of gravity-driven movement on passive margins: Quantifying the relative contribution of spreading vs. gravity sliding mechanisms. *Tectonophysics*, 633, 126–142.
<https://doi.org/10.1016/j.tecto.2014.06.023>

- Prather, B. E., Pirmez, C., Sylvester, Z., & Prather, D. S. (2012). Stratigraphic response to evolving geomorphology in a submarine apron perched on the upper Niger Delta slope. In B. E. Prather, M. E. Deptuck, D. Mohrig, B. van Hoorn, & R. Wynn (Eds.), *Application of the principles of seismic geomorphology to continental-slope and base-of-slope systems: Case studies from seafloor and near-seafloor analogues* (Vol. 99, pp. 347–369). SEPM, Special Publication.
- Ramberg, H. (1981). *Gravity, deformation and the Earth's crust in theory, experiments and geological application* (2nd ed., p. 452). Academic Press.
- Restrepo-Pace, P. (2018). 'Ductile v. Brittle'-alternative structural interpretations for the Niger Delta. *Geological Society of London Special Publication*, 46, 1–12.
- Robin, C., Guillocheau, F., Jeanne, S., Porcher, F., & Calves, G. (2011). Cenozoic siliciclastic fluxes evolution around Africa. *Geophysical Research Abstracts*, 13, EGU2011-5659.
- Rouby, D., Nalpas, T., Jermannaud, P., Robin, C., Guillocheau, F., & Raillard, S. (2011). Gravity driven deformation controlled by the migration of the delta front: The Plio-Pleistocene of the Eastern Niger Delta. *Tectonophysics*, 513, 54–67. <https://doi.org/10.1130/GEOSO1426.1>
- Rowan, M. G., Peel, F. J., & Vendeville, B. C. (2004). Gravity-driven fold belts on passive margins. In K. R. McClay (Ed.), *Thrust tectonic and hydrocarbon systems*, AAPG Memoir (Vol. 82, pp. 157–182).
- Sapin, F., Ringenbach, J.-C., Rives, T., & Pubellier, M. (2012). Counterregional faults in shale-dominated deltas: Origin, mechanism and evolution. *Marine and Petroleum Geology*, 37, 121–128.
- Schultz-Ela, D. (2001). Excursus on gravity gliding and gravity spreading. *Journal of Structural Geology*, 23(5), 725–731. [https://doi.org/10.1016/S0191-8141\(01\)00004-9](https://doi.org/10.1016/S0191-8141(01)00004-9)
- Séranne, M., & Nzé Abeigne, C. R. (1999). Oligocene to Holocene sediment drifts and bottom currents on the slope of Gabon continental margin (west Africa): Consequences for sedimentation and southeast Atlantic upwelling. *Sedimentary Geology*, 128, 179–199.
- Short, K. C., & Stauble, A. J. (1967). Outline of geology of Niger Delta. *AAPG Bulletin*, 51, 761–779. <https://doi.org/10.1306/5D25C0CF-16C1-11D7-8645000102C1865D>
- Wiener, R. W., Mann, M. G., Angelich, M. T., & Molyneux, J. B. (2010). Mobile shale in the Niger Delta: Characteristics, structure, and evolution. In L. Wood (Ed.), *Shale tectonics* (Vol. 93, pp. 145–161). American Association of Petroleum Geologists (AAPG) Memoir.
- Willett, S. C. (2010). Late Neogene erosion of the Alps: A climate driver? *Annual Review of Earth and Planetary Science*, 38, 37–411. <https://doi.org/10.1146/annurev-earth-040809-152543>
- Wu, J. E., McClay, K., & Frankowicz, E. (2015). Niger Delta gravitydriven deformation above the relict Chain and Charcot fracture zones, Gulf of Guinea: Insights from analogue models. *Marine and Petroleum Geology*, 65, 43–62

Figure 1: Location of the study area. (a) Location of the Niger Delta in the Gulf of Guinea in west Africa, offshore fracture zones and volcanic lines. (b) Superposed relief and bathymetry map of the Niger Delta showing the extensional zone (EZ), translational zone (TZ), contractional zone (CZ) and the abyssal plain (AP) (modified after Rouby et al., 2011). The light green and red lines on panel B represent local and regional 2D seismic lines, respectively. Red circles show well locations on the continental shelf (FMSL 1–5). The blue box and blue circles, show 3D seismic coverage, and well locations, respectively on the continental slope (IZSH 1–15). (c) Regional line drawing, showing the structural styles of the offshore western Niger Delta (modified after Bellingham et al., 2014). (d) A schematic illustration of the lithostratigraphic units underlying the Niger Delta (modified after Corredor et al., 2005). See text for a more detailed explanation

Figure 2: Plot of average velocity (m/s) versus measured depth (m) extracted from the checkshot data of the deepest FMSL 1 well, used for depth conversion. See text for a more detailed explanation.

Figure 3: Interpreted, regional seismic line (depth) (see Figure 1b for location), showing the presence of landward-dipping top of basement (TB), and regional detachment (RD), underlain by lower detachment unit (LDU), and overlain by upper detachment unit (UDU). Note: (i) the listric geometry of normal faults, and their general termination on RD, (ii) undulating geometry of late Eocene to Tortonian surfaces, and (iii) a general increase in sediment thickness within the extensional zone from the early Pliocene to present. See text for a more detailed explanation

Figure 4 (a, b): Interpreted regional seismic line and line drawing (depth), showing the tectono-stratigraphic architecture of the offshore WNDL (see Figure 1b for location). Note: (i) the listric geometry of normal faults within deeper stratigraphic intervals, and their general termination on RD, (ii) undulating geometry of late Eocene to Serravallian surfaces, and (iii) a general increase in sediment thickness within the extensional zone from the early Pliocene to present. For more details, see zoomed sections outlined in red boxes in panel A (c–f). (c) Detailed view of the extensional zone, showing the incisional character of the early Pliocene, and an overall thickening in stratigraphy. (d) Detailed view of the translational zone, showing (i) the presence of BH (barrier), formed by thrust/shale-cored anticline, characterised by headwall scars at the shelf-slope break, (ii) an overall thinning of stratigraphy above BH, and concomitant thickening within adjacent piggyback basin, (iii) incisional character of the early Pliocene surface, and (iv) undulating geometry of the late Eocene/Serravallian surface below duplexes. (e) Detailed view of the IFTB, showing thrust/shale-cored anticlines, flanked by piggyback/intraslope basins. Note: (i) the presence of headwall scars above the bathymetric surface to the right, that are flanked by MTDs, (ii) the general thinning of stratigraphy above bathymetric high,

and a corresponding thickening within piggyback basins, and (iii) the incisional character of the Tortonian, early Pliocene and early Pleistocene surfaces above bathymetric high to the left. (f) Detailed view of the OFTB, showing (i) the detachment of reverse faults on RD, (ii) a general thinning/onlapping of stratigraphy above thrust/shale-cored anticlines, and a corresponding thickening within piggyback basins, (iii) the incisional character of the early and middle Pleistocene surfaces. See text for a more detailed explanation.

Figure 5: (a, b) Interpreted regional seismic line and line drawing (depth) (see Figure 1b for location). Note: (i) the listric geometry of normal faults within deeper stratigraphic intervals, and their general termination on RD, (ii) undulating geometry of late Eocene to early Pleistocene surfaces, (iii) a general increase in sediment thickness within the extensional zone from the early Pliocene to present. See text for a more detailed explanation

Figure 6 (a, b): Interpreted and seismic line drawing of the delta-wide strike line (TWT), located on the shelf (Figure 1b). Note: (i) the presence of paleo-topographies, formed by the Charcot and Chain Fracture Zones in the central and western Niger Delta, respectively, and the occurrence of listric normal faults above them, (ii) lateral variation in sediment thickness over the Cretaceous-Serravallian, with overall thinning above the relict fracture zones, and thickening on the flanks, the general thinning of the early Pliocene-present Unit from the ENDL to WNDL. For more details, see below, zoomed sections of the areas outlined in red boxes in panel B (c–e). (c) Detailed view of the ENDL, showing an overall thickening of the early Pliocene-present Unit. (d) Detailed view of the relief, formed by the relict Charcot Fracture Zone. Note the presence of listric normal faults, and an overall thinning of the Cretaceous-Serravallian Unit above the paleotransform. (e) Detailed view of the relief, formed by the relict Chain Fracture Zone in the WNDL. Note the presence of listric normal faults, and an overall thinning of stratigraphy above the paleo-transform

Figure 7 (a, b): Estimated average sediment thickness (km), and sedimentation rates (km/Ma) on the offshore WNDL. Note the general increase in average sediment thickness/deposition rate from the late Eocene to the Tortonian, slight decrease from the Tortonian to the early Pliocene, and onwards increase from the early Pliocene to present

Figure 8: Schematic illustration of the tectono-stratigraphic evolution of the offshore western Niger Delta from the Cretaceous to the Present. (a) Development of duplexes within the upper detachment unit; (b) initiation of gravity-driven deformation within the currently active extensional and translational zones; (c) coupling of deformation between the extensional and translational zones, and

inferred progradation of the 'Oligocene-Tortonian extensional zone'; (d) acceleration of gravity-collapse of the continental shelf, and initiation of deformation within the OFTB; (e) intensification of gravity collapse and deformation at the leading front of the OFTB

Figure 9 (a) Location of the 'Oligocene-Tortonian extensional zone' on the present onshore. (b) Basinward progradation of the 'Oligocene-Tortonian extensional zone'. (c) Modern Niger Delta extensional, translational and contractional zone

Figure 10 (a, b) Line drawing, showing the stratigraphic architecture of the offshore ENDL (after Jermannaud et al., 2010) and WNDL. Note: (i) Overall progradation during the late and early Pliocene, in the ENDL and WNDL; (ii) retrogradation and sediment storage on shelf of the ENDL in the Pleistocene, compared to progradation and sediment bypass on the shelf of WNDL during the Pleistocene

Table 1: Summary of the seismic and borehole data used in this study

Seismic	Type	Area (km ²)	Polarity	Phase	Frequency (Hz)	Sampling interval (ms)	Vertical resolution (m)
Shelf	2D	4,120	American	Zero phase	15–20	4	13.7–25
Slope	3D	638	reversed		25–30	4	25–30
Well	GR	RES	NEU	DEN	DT	Checkshot	Biostratigraphy
IZSH 1	✓	✓	x	✓	✓	✓	✓
IZSH 2	✓	✓	x	✓	✓	✓	x
IZSH 3	✓	✓	x	✓	✓	x	x
IZSH 4	✓	✓	x	✓	✓	✓	x
IZSH 5	✓	✓	x	✓	✓	x	x
IZSH 6	✓	✓	x	✓	✓	✓	x
IZSH 7	✓	✓	x	x	✓	✓	✓
IZSH 8	✓	✓	x	x	x	x	x
IZSH 9	✓	✓	x	✓	✓	x	x
IZSH 10	✓	✓	x	✓	✓	x	x
IZHS 11	✓	✓	✓	✓	✓	✓	✓
IZSH 12	✓	✓	x	x	x	x	x
IZSH 13	✓	✓	x	✓	✓	✓	x
IZSH 14	✓	✓	x	✓	✓	✓	x
IZSH 15	✓	✓	x	✓	✓	✓	x
FMSL 1	✓	✓	✓	✓	✓	✓	✓
FMSL 2	✓	✓	✓	✓	✓	✓	✓
FMSL 3	✓	✓	✓	✓	✓	✓	✓
FMSL 4	✓	✓	✓	✓	✓	✓	✓
FMSL 5	✓	✓	✓	✓	✓	✓	x

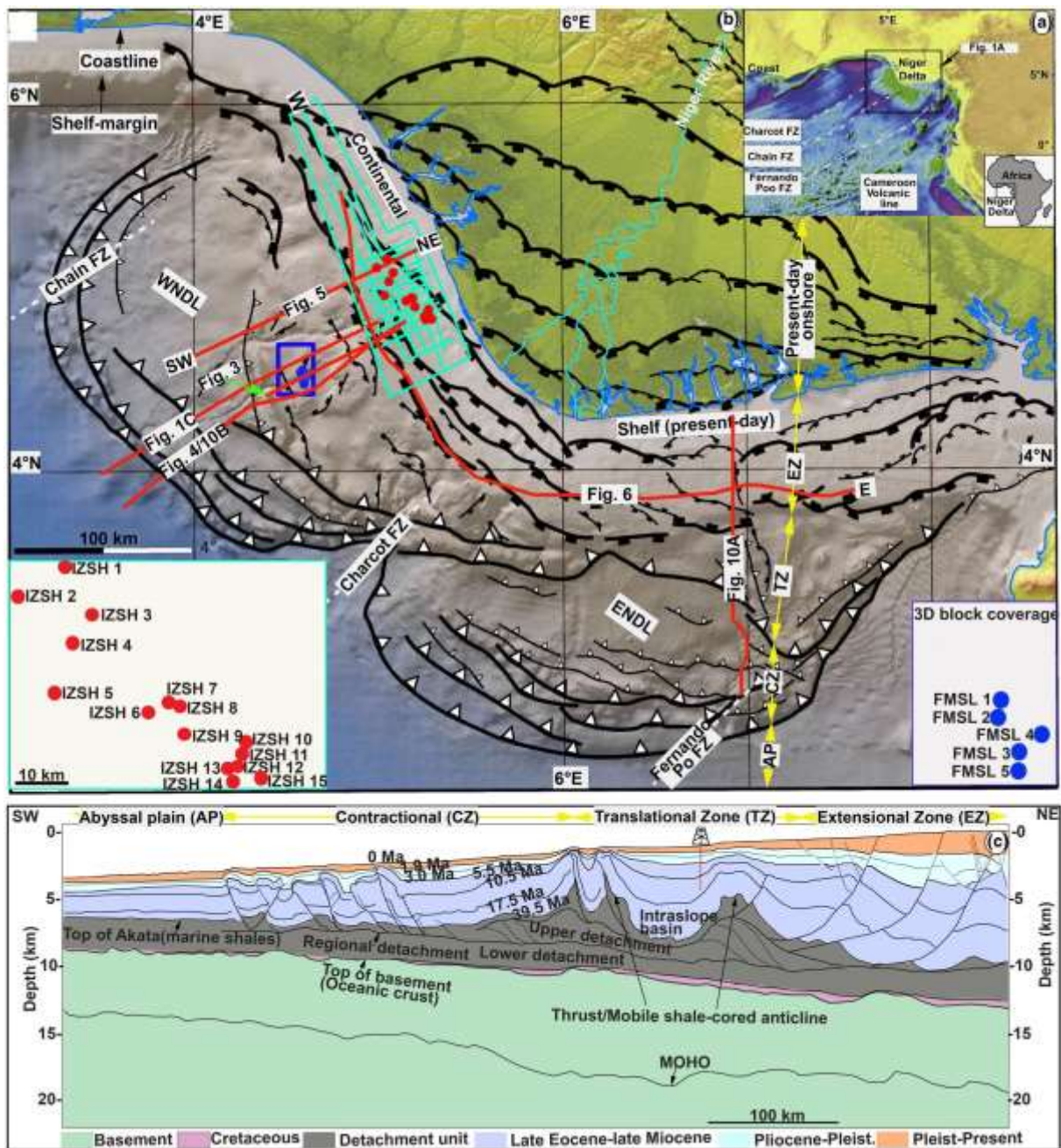


Figure 1 (a,b,c)

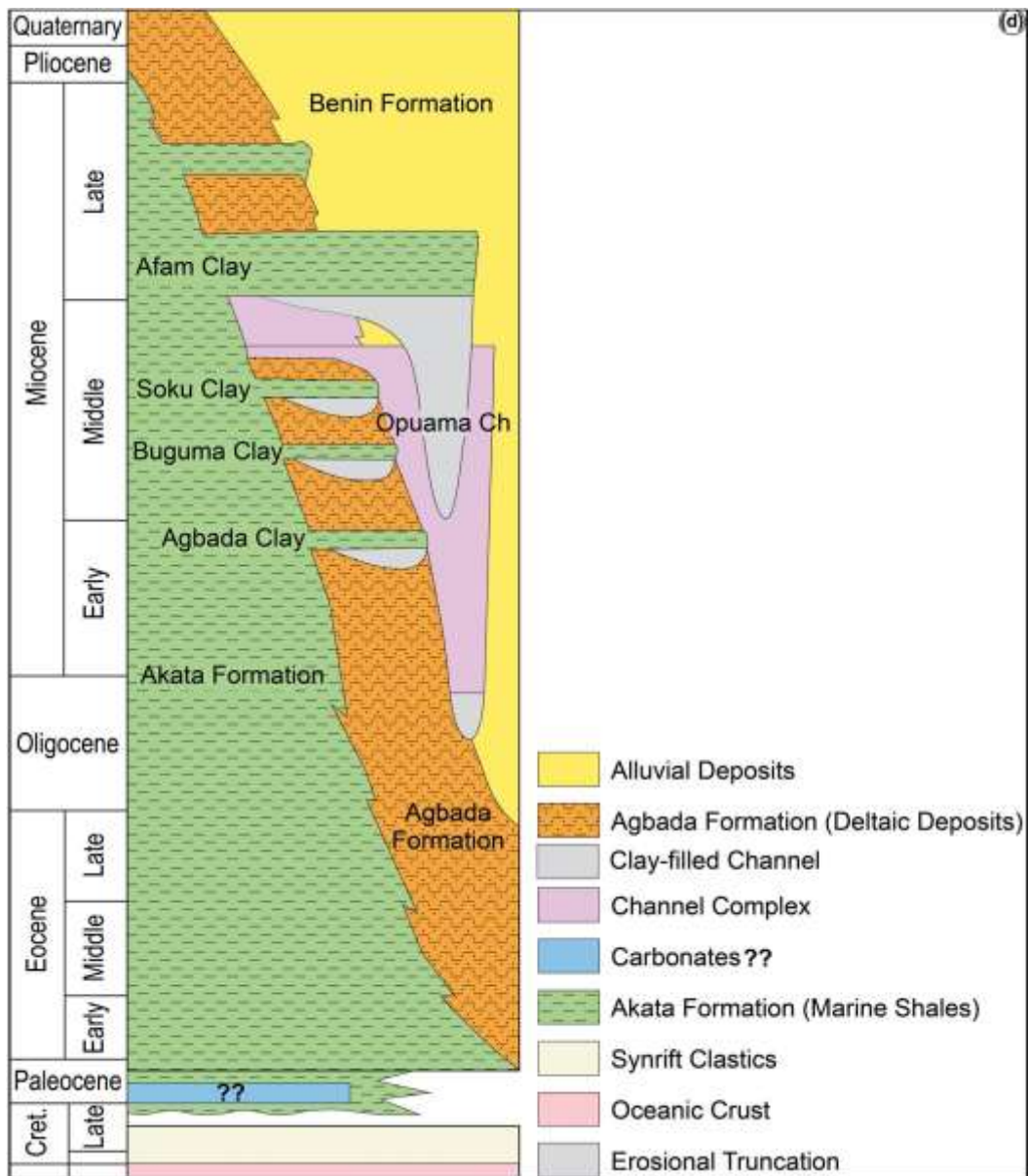


Figure 1 (d)

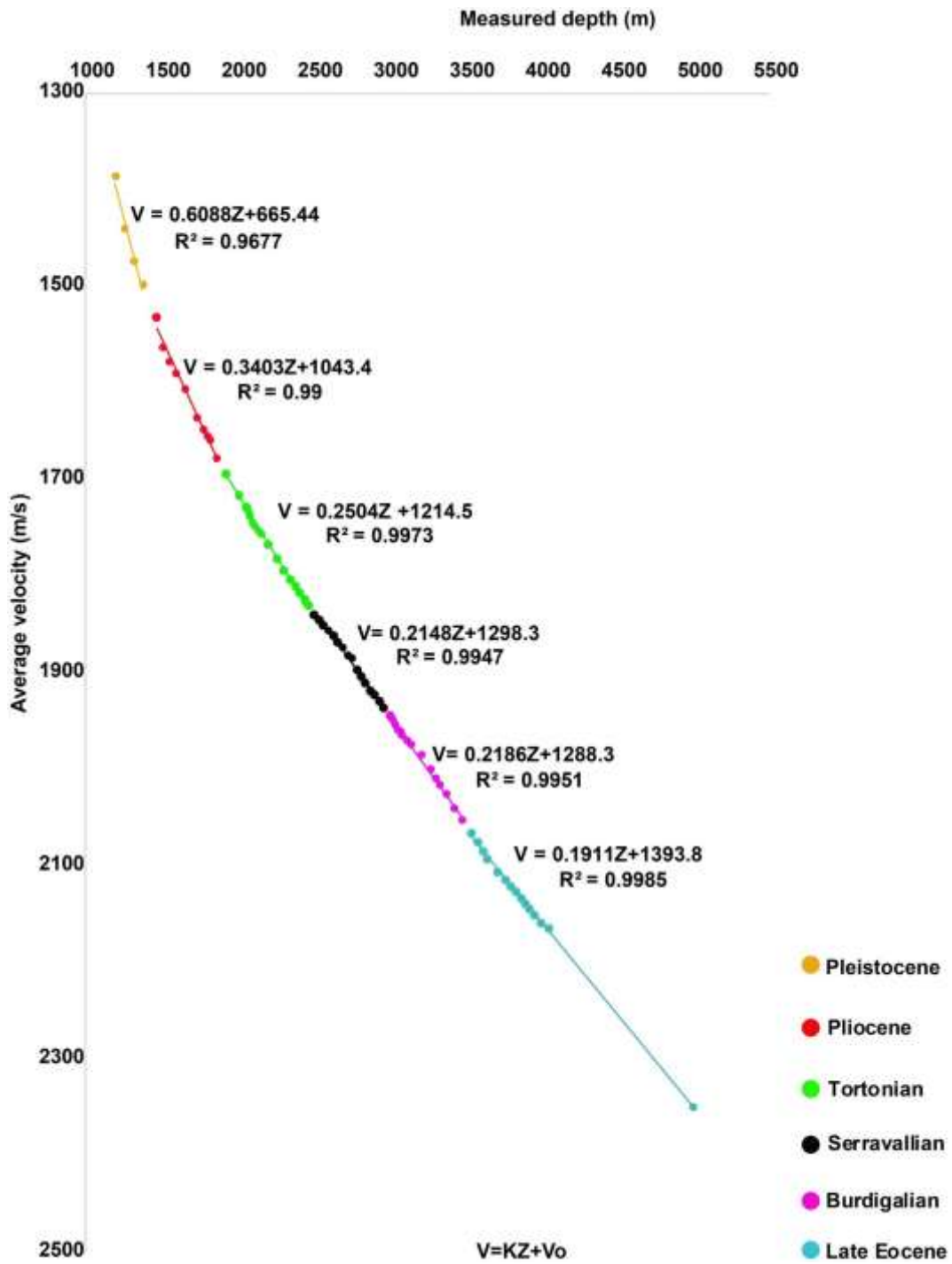


Figure 2

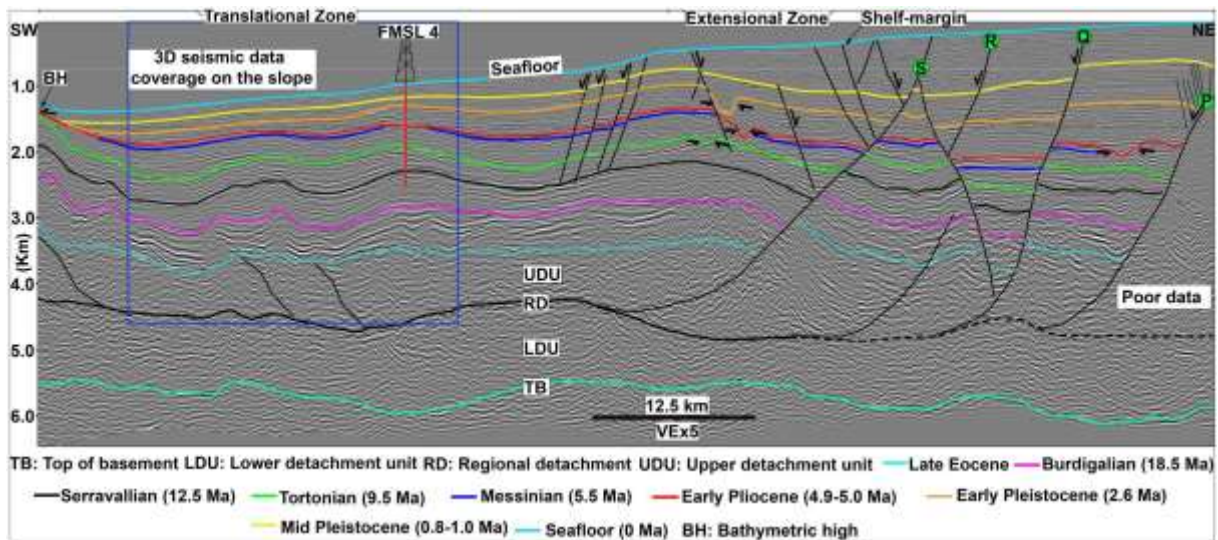


Figure 3

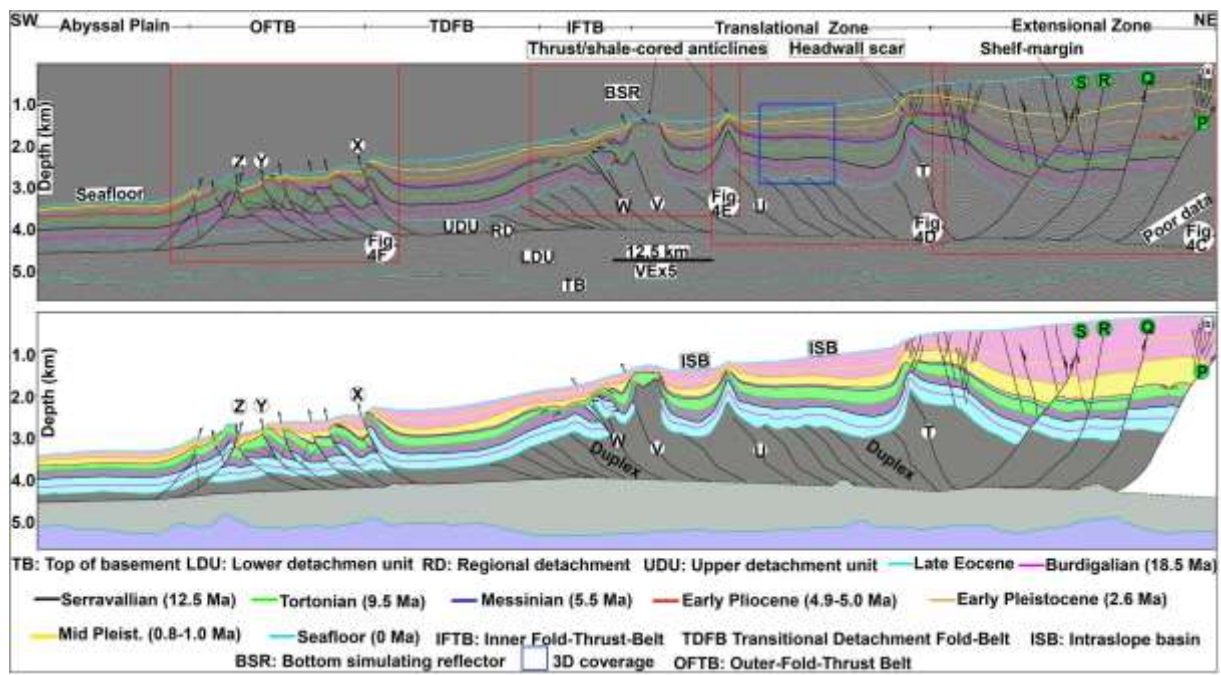


Figure 4 (a,b)

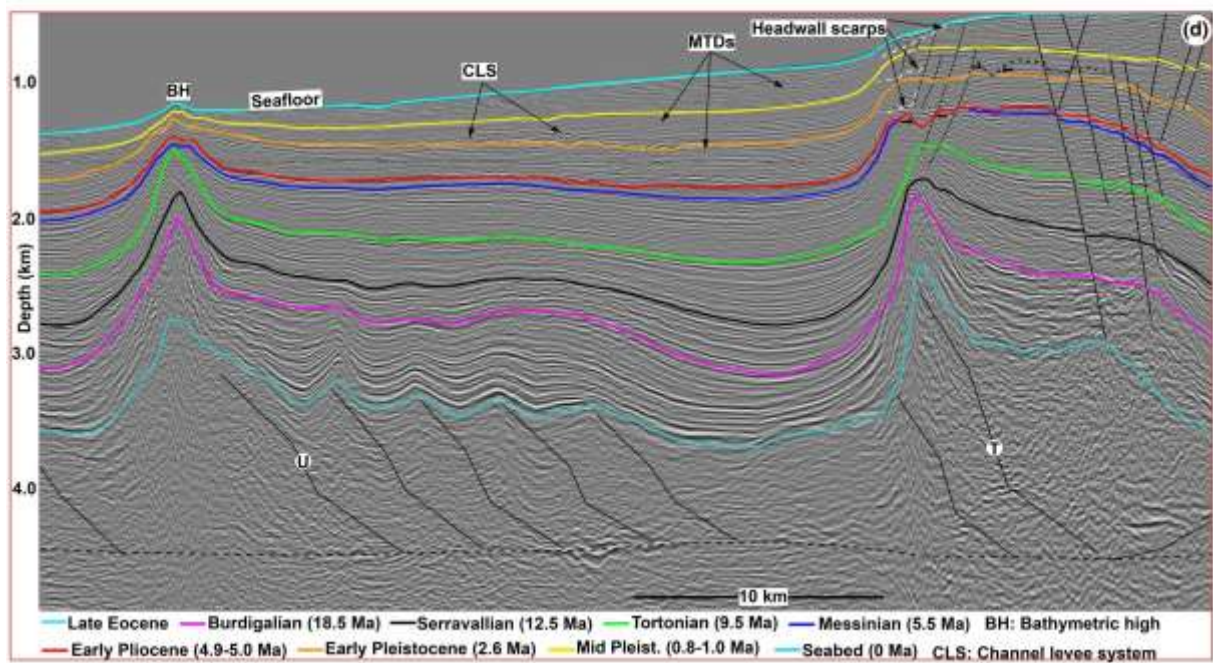
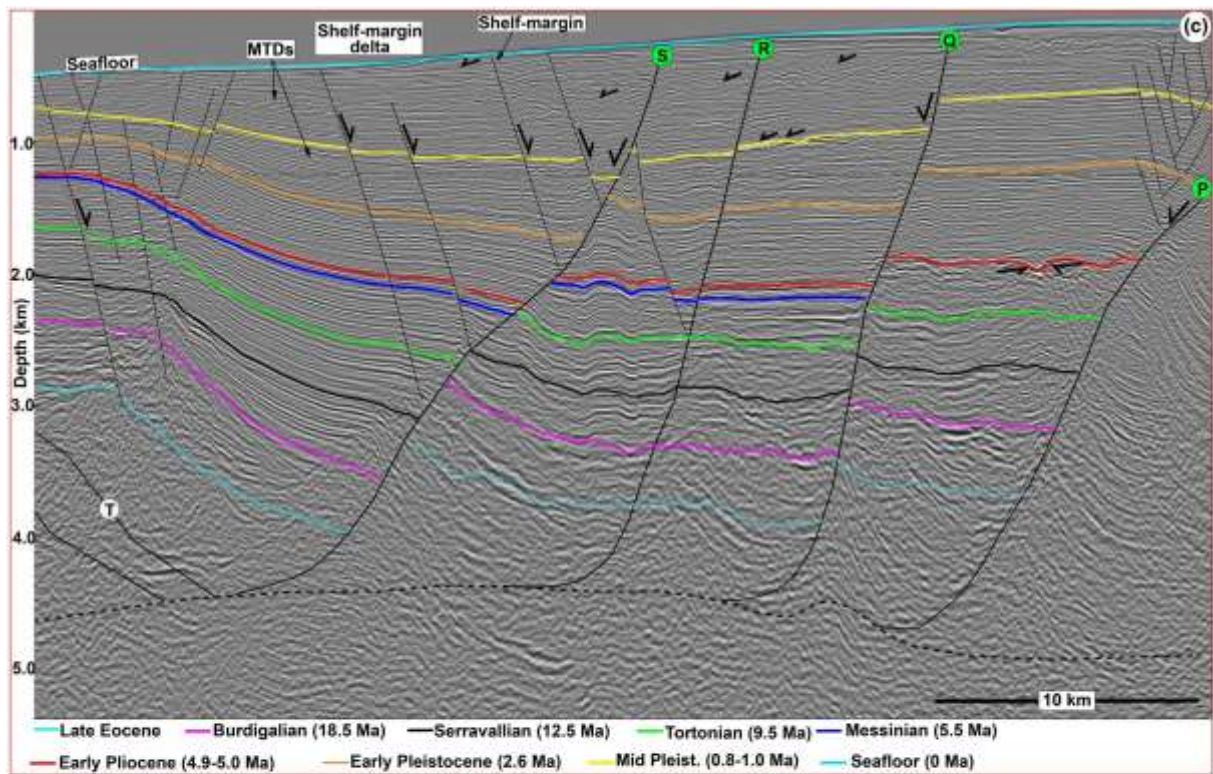


Figure 4 (c,d)

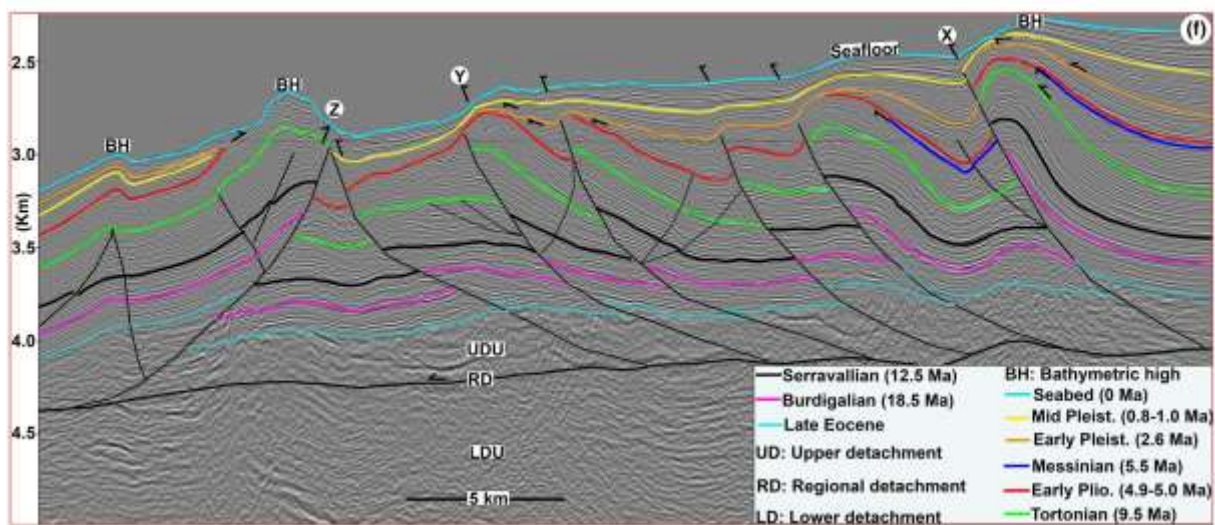
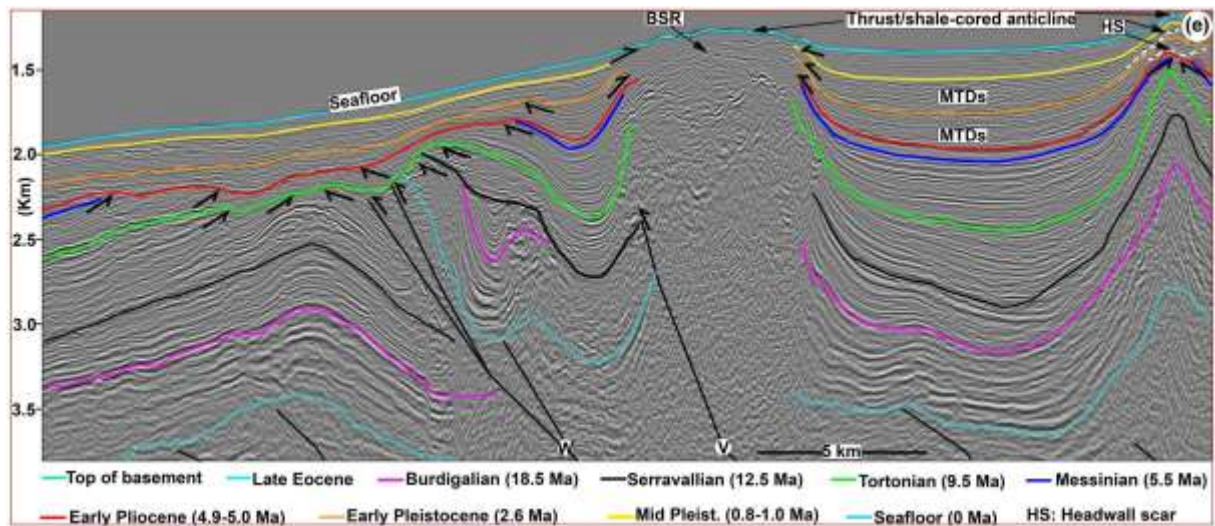


Figure 4 (e,f)

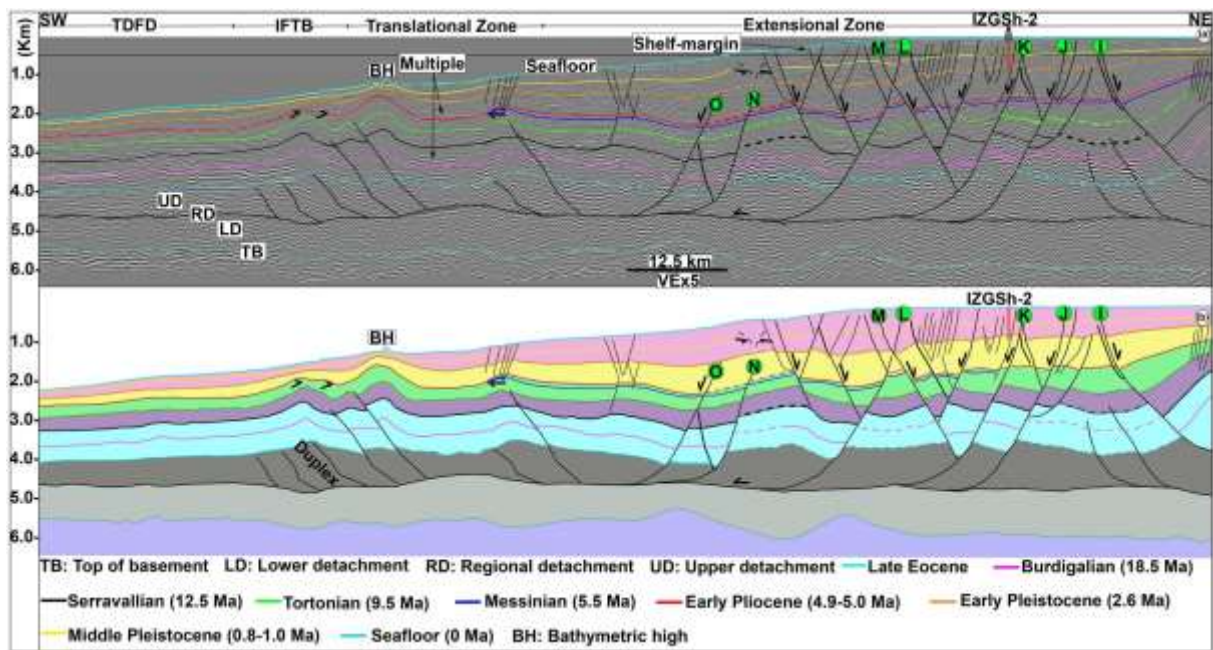


Figure 5

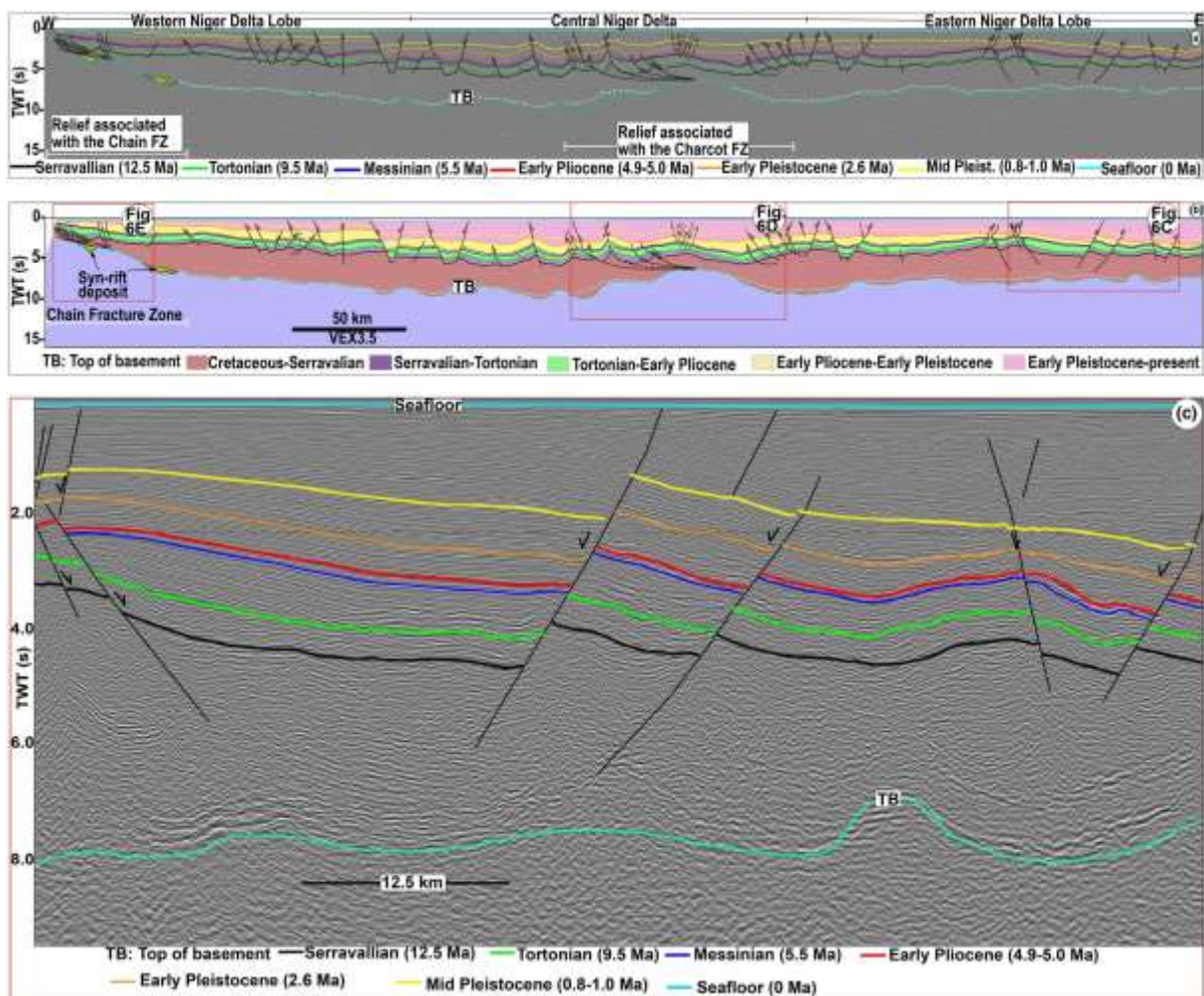


Figure 6 (a,b,c)

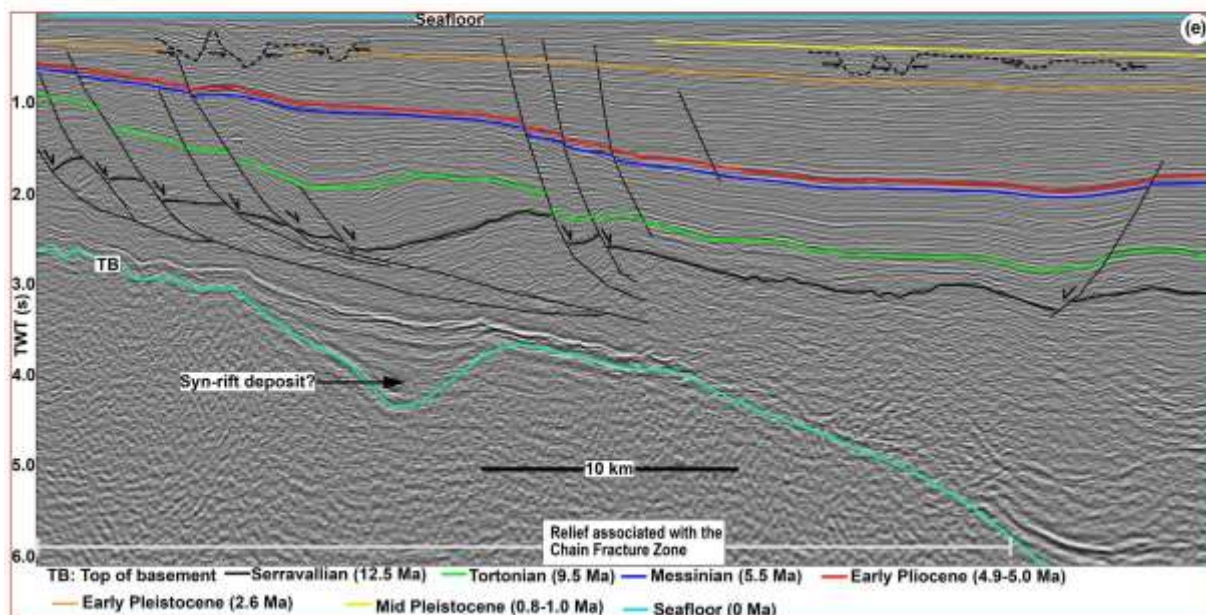
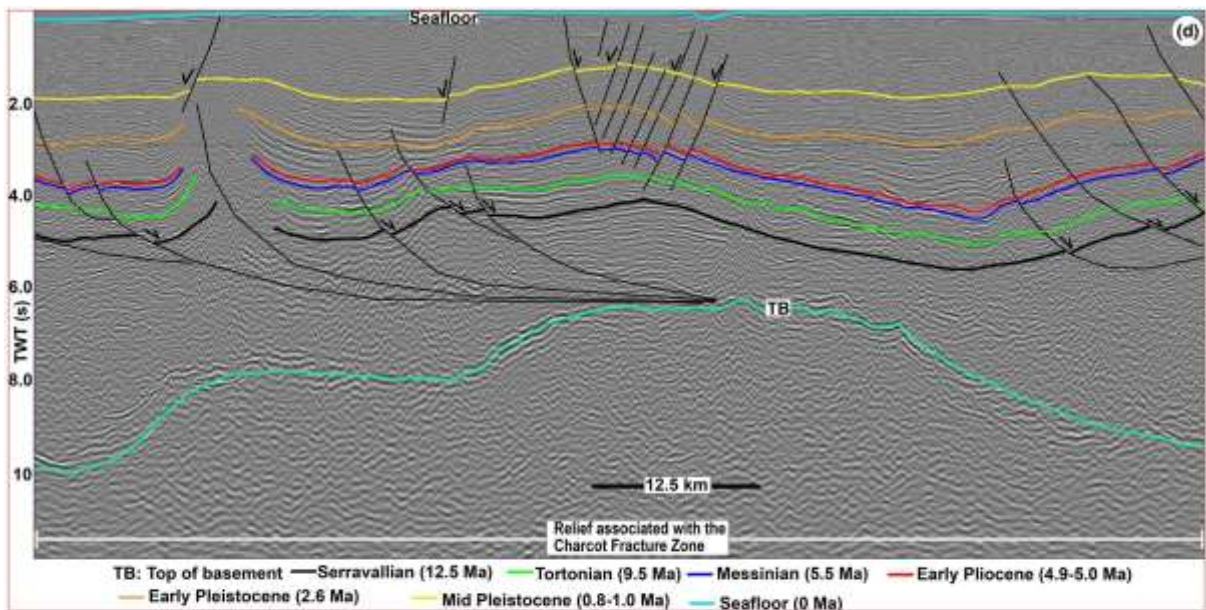


Figure 6 (d,e)

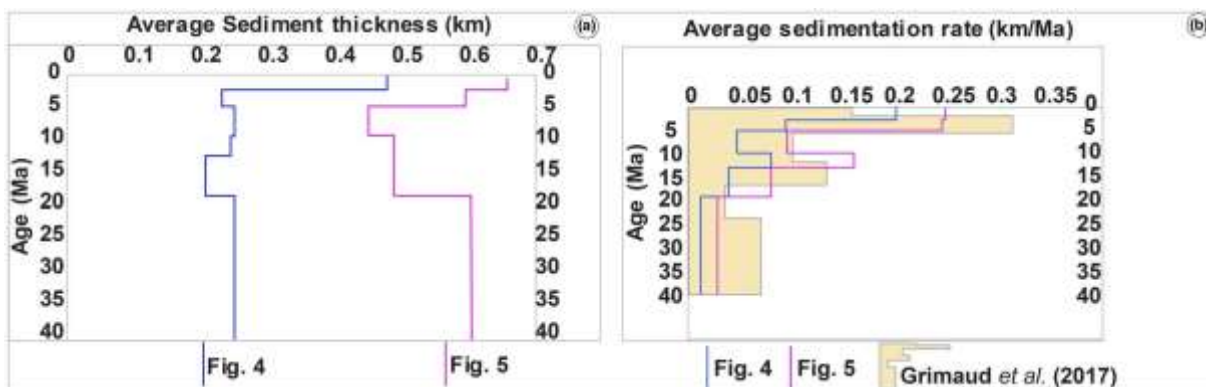


Figure 7

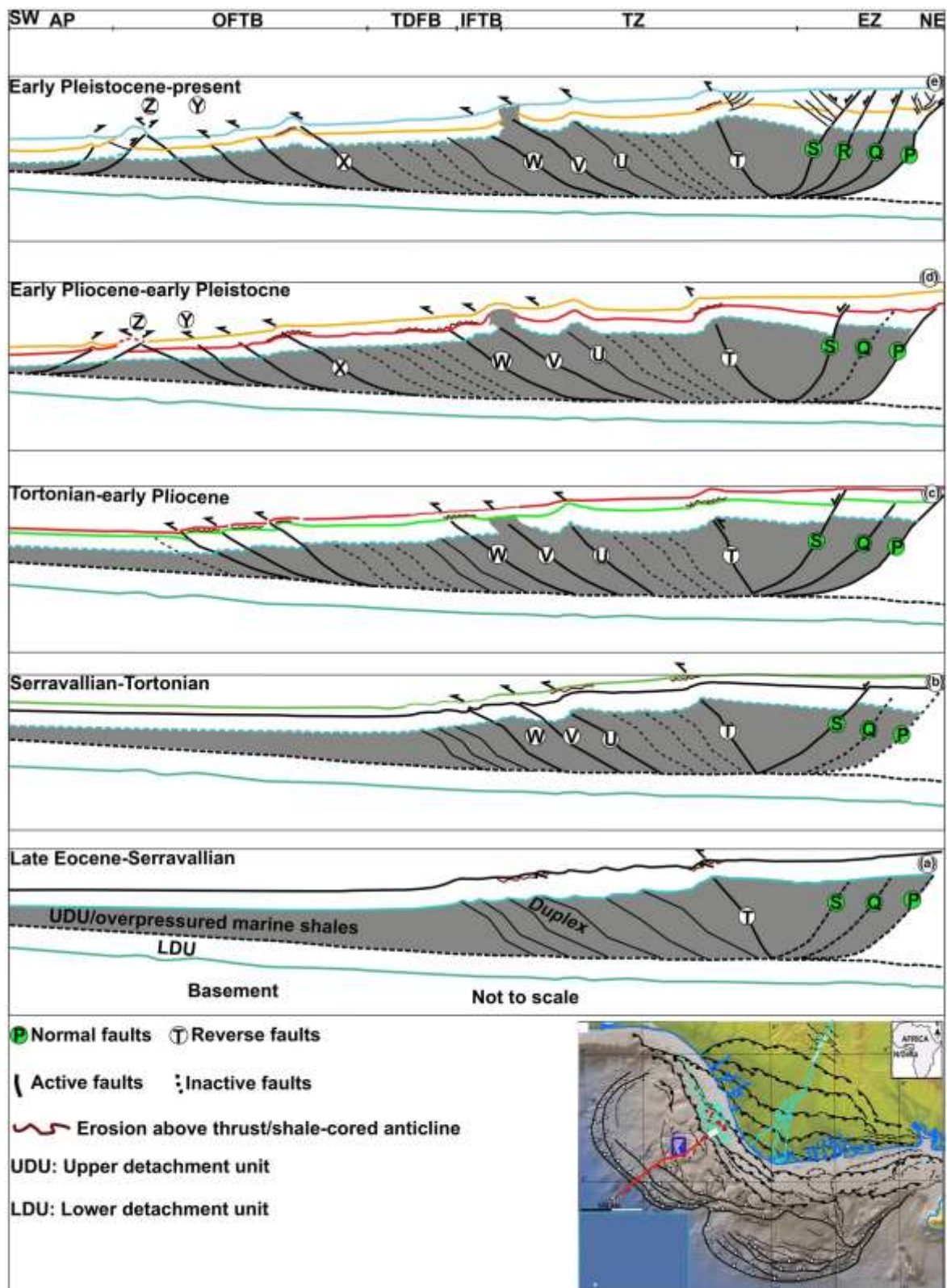


Figure 8

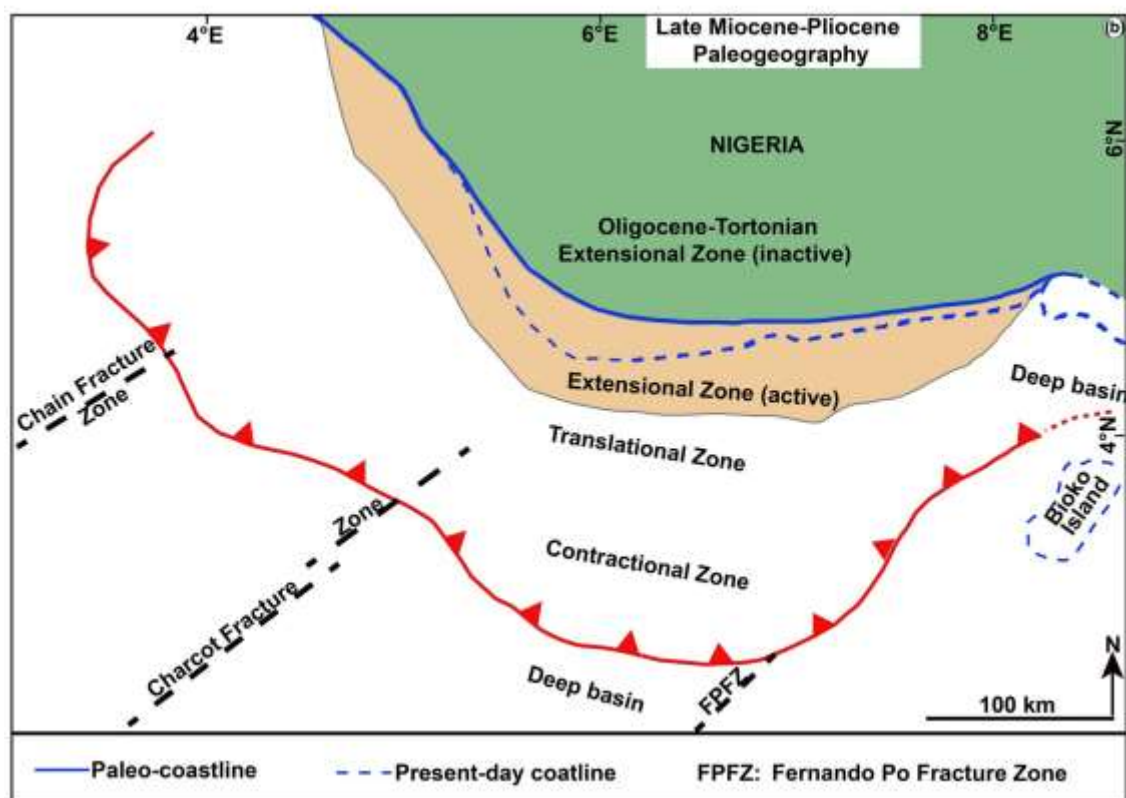
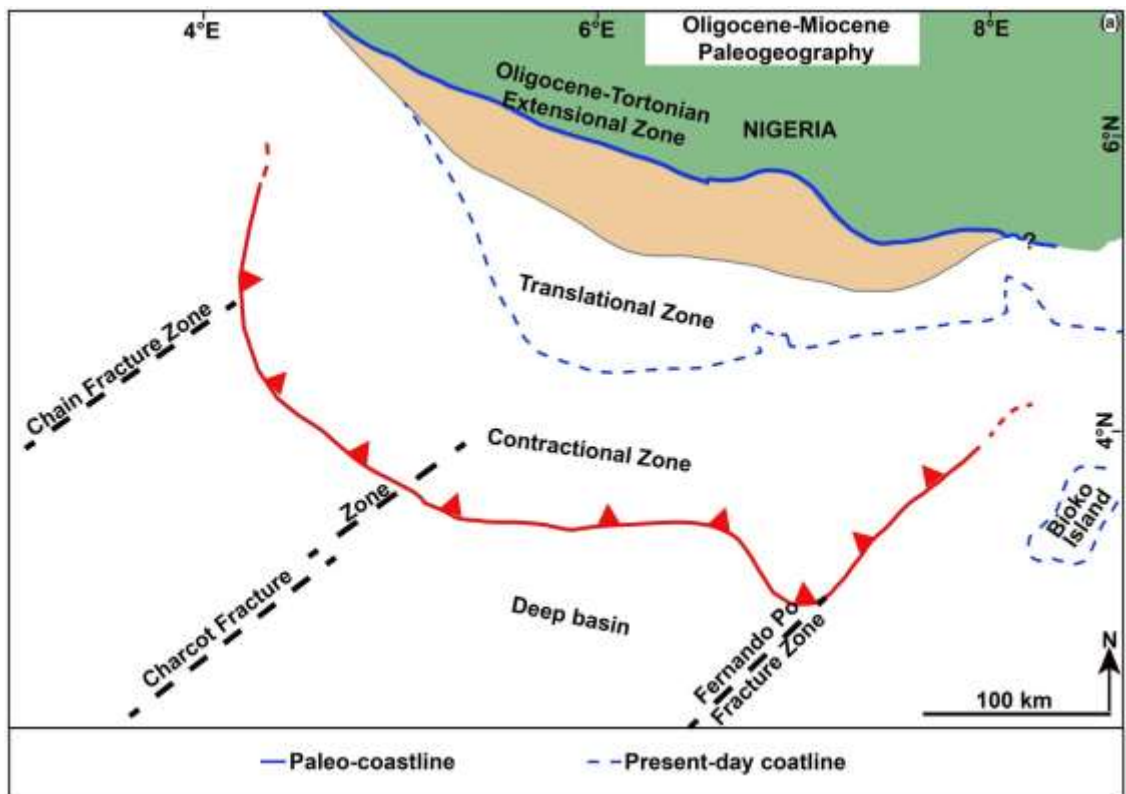


Figure 9 (a,b)

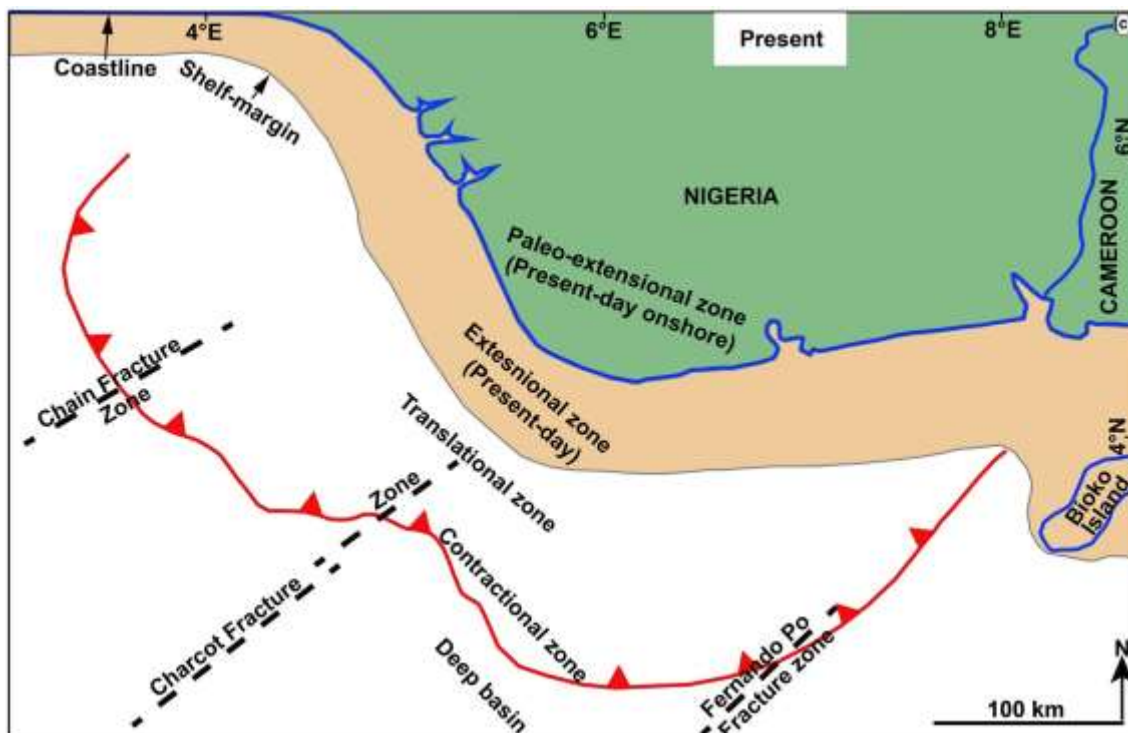


Figure 9 (c)

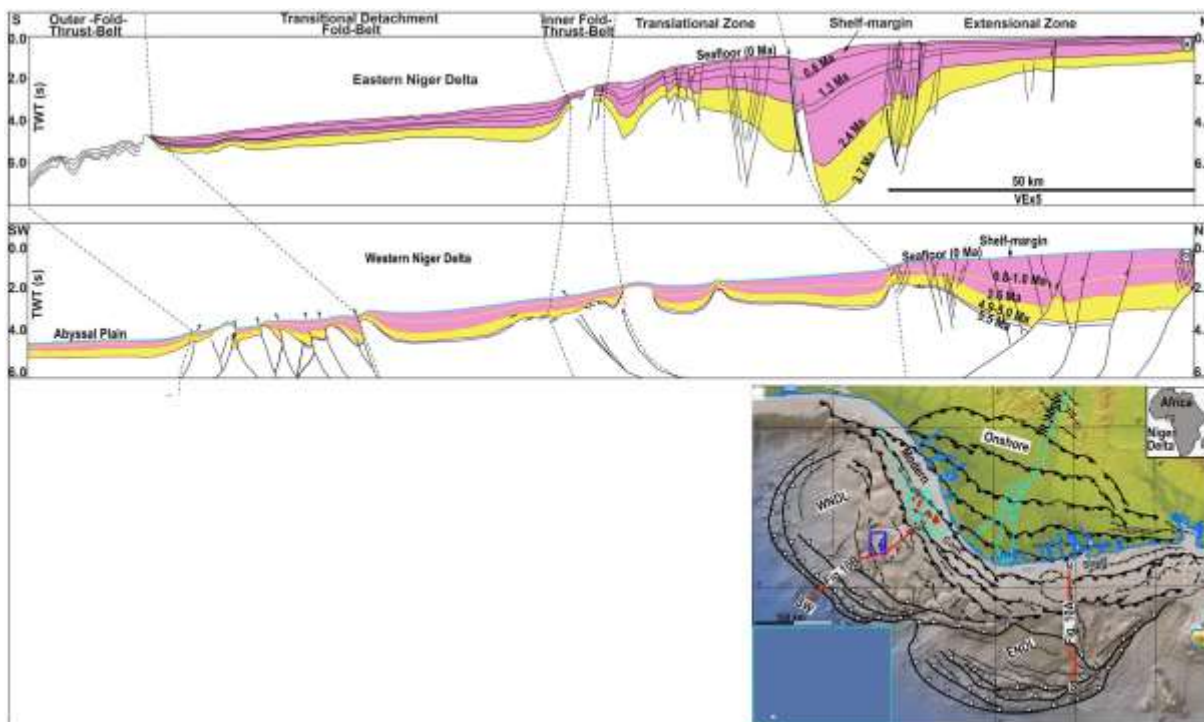


Figure 10